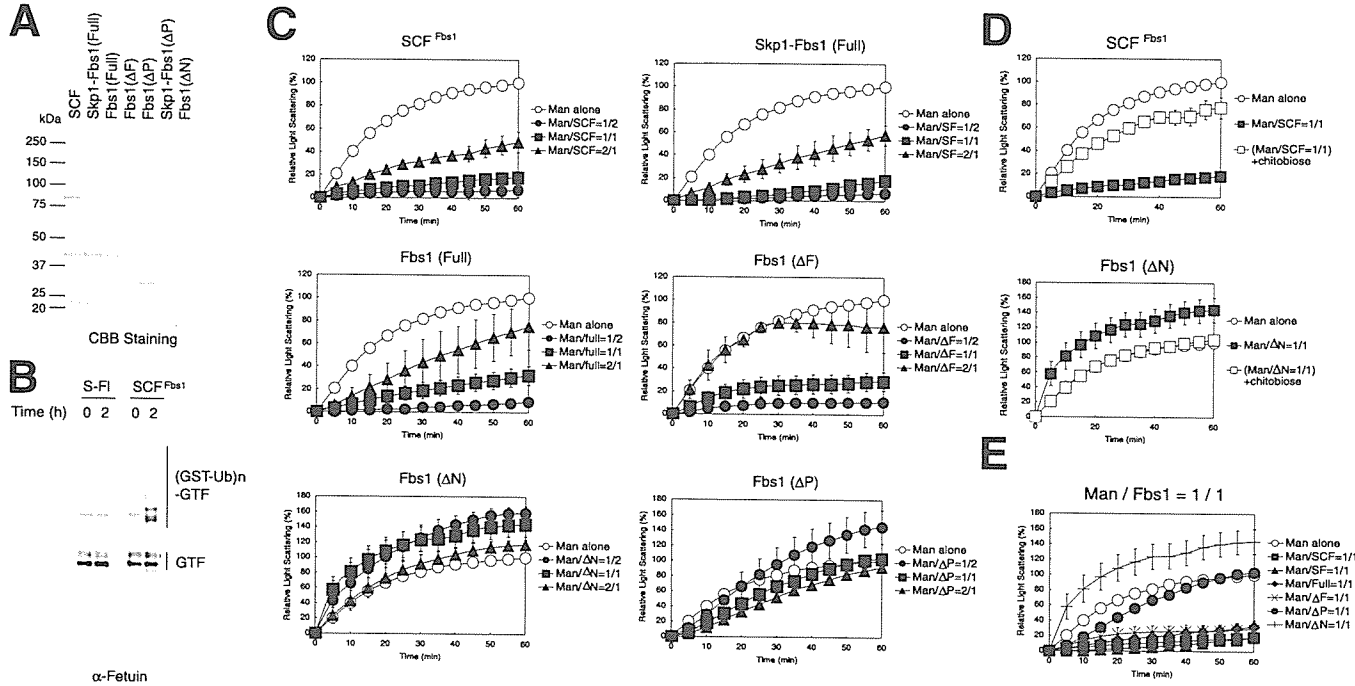

FIGURE 5. **Fbs1 complexes suppress the aggregation of denatured α-mannosidase *in vitro*.** *A*, electrophoretic pattern of the recombinant proteins produced by the baculovirus system. *CBB Staining*, Coomassie Brilliant Blue staining. *B*, GlcNAc-terminated fetuin (*GTF*) was incubated in a reaction mixture containing the ATP-regenerating system, recombinant ubiquitin-activating enzyme (E1), Ubc4, GST-ubiquitin (*GST-Ub*), and Skp1-Fbs1 dimer (*S-Fl*) or SCF complex (*SCF*) in the presence of the NEDD8 system at 30 °C. The high molecular mass ubiquitylated fetuin ((*GST-Ub*)*n-GTF*) was detected by immunoblotting with anti-fetuin antibody. *C*, after denaturation in 6 M GdnHCl, α-mannosidase (*Man*) was diluted to a final concentration of 0.3 mM at 25 °C in the presence of the indicated concentrations of SCF^{Fbs1} (SCF^{Fbs1} or *SCF*), Skp1 and Fbs1 dimer (*Skp1-Fbs1 (Full)* or *SF*), Fbs1 monomer (*Fbs1 (Full)* or *Full*), or Fbs1 derivatives (Δ*F*, Δ*N*, or Δ*P*). Aggregation was measured by monitoring light scattering at 360 nm over a period of 60 min. Data are the mean ± S.D. of at least three independent experiments. *D*, α-mannosidase was allowed to aggregate in the presence of equal mole of SCF^{Fbs1} or Fbs1 (ΔN). 0.05 mM *N*, *N*′-diacetylchitobiose was added (+chitobiose), and the effects on aggregation were monitored by measuring light scattering at 360 nm. Data are the mean and standard deviation of three independent experiments. *E*, α-mannosidase was allowed to aggregate in the presence of equal mole of recombinant Fbs1 complexes or derivatives. Data are the mean ± S.D. of three independent experiments.

Fbs1 derivatives. The degradation of P23H was suppressed by MG132 treatment as reported previously (Fig. 4*B*). Although wild-type Fbs1 or the YW mutant did not influence the kinetics of P23H degradation, co-expression of Fbs-2N1C efficiently promoted its degradation. On the other hand, like wild-type Fbs1, Fbs1 I2, could associate with P23H, but its expression did not influence both the amount of P23H and the kinetics of P23H degradation (data not shown). These results demonstrate that the non-SCF complex of Fbs1 can be converted to an active E3 ligase by introducing the complex-forming activity mapped onto the F-box domain and the linker sequence of Fbs2.

Fbs1 Suppresses Aggregation of Denatured Glycoprotein in Vitro—We reported previously that the expression of Fbs1 inhibits aggresome formation in Cos7 cells (8). Furthermore, since Fbs1 interacts with denatured glycoproteins more efficiently than native glycoproteins, we examined whether Fbs1 functions as a molecular chaperone for glycoproteins *in vitro*. To this end, we prepared recombinant SCF^{Fbs1}, Skp1-Fbs1 dimers, Fbs1, Fbs1 ΔF, Fbs1 ΔP, Skp1-ΔP dimers, and Fbs1 ΔN, all of which were produced by using a baculovirus system (Fig. 5*A*). To obtain highly purified recombinant proteins, we purified them by using the affinity for the RNaseB resin but not nickel resin toward His tag. The purified SCF^{Fbs1} but not Skp1-Fbs1 dimers could ubiquitylate GlcNAc-terminated fetuin (*GTF*) effectively (Fig. 5*B*). We next assessed the ability of these proteins or their complexes to suppress the aggregation by using denatured α-mannosidase that contains high mannose type oligosaccharides, a typical substrate for the glycoprotein aggregation assay (17). Although Fbs1 alone suppressed the aggregation of denatured α-mannosidase in a concentration-dependent manner, the Fbs1-Skp1 dimers as well as the SCF^{Fbs1} complex suppressed the aggregation much more effectively than Fbs1 alone (Fig. 5*C*). Although the addition of half-molar of Fbs1 ΔF did not affect the aggregation of denatured α-mannosidase, ΔF was also active to suppress the aggregation at a level similar to that of Fbs1 alone in an equal molar ratio, suggesting that the partial suppression by Fbs1 is independent of the hydrophobic F-box domain. On the other hand, ΔN, consisting of substrate-binding domain alone, enhanced its aggregation. Both the aggregation-suppressing activity of SCF^{Fbs1}, Skp1-Fbs1 dimers, or Fbs1 and the aggregation-enhancing activity of ΔN were inhibited by chitobiose (Fig. 5*D* and not shown). In contrast, these recombinant Fbs1 protein complexes had no effect on the aggregation of non-glycosylated proteins such as citrate synthase and luciferase (data not shown). Importantly, ΔP as well as the Skp1-ΔP dimers could not suppress the aggregation of α-mannosidase in an equal molar ratio (Fig. 5, *C* and *E*, and not shown). These results indicate that the Skp1-Fbs1 dimers effectively suppress the aggregation of denatured glycoproteins by recognizing the exposed chitobiose in *N*-glycans and that the P domain of Fbs1 is required for this aggregation suppressing activity.

DISCUSSION

The F-box family of proteins, which are the substrate-recognition subunits of the SCF ubiquitin ligase, play important roles in ubiquitin-dependent proteolysis in eukaryotes (18, 19). However, it is not clear whether all F-box proteins indeed function as receptor subunits of SCF complexes. For example, it has been reported that at least two F-box proteins, Ctfl3 and Rcy1, out of 11 F-box proteins in *Saccharomyces cerevisiae*, do not form SCF complexes (20–22). Since not all RING-finger proteins are ubiquitin ligases, it is possible that non-canonical F-box proteins that fail to form the SCF complex play some important roles other than ubiquitin ligase activity. In the present study, we showed that the SCF complex formation of Fbs1, which recognizes *N*-glycans, is not efficient and that the intervening segment between the F-box domain and the sugar-binding domain of Fbs1 suppresses the formation of the SCF complex. The major population of Fbs1 is present as Fbs1-Skp1 heterodimers or Fbs1 monomers, which can inhibit the aggregation of the glycoproteins. Our results show that Fbs1 contributes to a chaperone function in addition to the role of the SCF^{Fbs1} ubiquitin ligase, opening new perspectives for cellular activities of F-box proteins.

Although most endogenous Fbs1 was not assembled into the SCF^{Fbs1} complex, a minor population of Fbs1 was capable of forming the SCF^{Fbs1} complex in cells. Moreover, the SCF^{Fbs1} complex could be produced in insect cells by infection with the baculovirus, indicating that Fbs1 can intrinsically form the SCF complex. It is worth noting that the SCF^{Fbs1} was mainly present in the 100,000 × *g* precipitate fraction including the microsome (Fig. 2, *B* and *C*). It is not clear why the SCF^{Fbs1} is bound to the ER membrane, although it is plausible that it plays a pivotal role in the ERAD pathway. To examine how the SCF complex formation of Fbs1 was promoted *in vivo*, we treated Fbs1-expressing cells with ER stress inducers, such as thapsigargin and dithiothreitol or a proteasome inhibitor MG132. These treatments, however, did not affect the SCF complex formation (data not shown). Furthermore, although the interaction between Fbs1 and its substrate glycoproteins did not affect the SCF complex formation (Figs. 1*A* and 3*B*), we examined the effects of overexpression of p97/VCP, Fbs1 substrates, Skp1, or Cul1. No protein other than Cul1 accelerated the SCF^{Fbs1} formation not only in the 100,000 × *g* precipitate fraction but also in the cytosol (Fig. 2*A* and data not shown). Intriguingly, whereas Fbs1 and Skp1 were mainly located in the cytosol (100,000 × *g* supernatant fraction), Cul1 was detected not only in the cytosol but also in the 100,000 × *g* precipitate fraction (Figs. 2, *B* and *C*, and 3*C*), suggesting that Cul1 is recruited to the microsome membrane where the SCF^{Fbs1} complex will be assembled to ubiquitylate efficiently the *N*-linked glycosylated ERAD substrates.

Fbs1 belongs to a subfamily consisting of at least five homologous F-box proteins that contain a conserved FBA motif in their C termini (5, 6). Among them, at least Fbs2 recognizes high mannose oligosaccharides as well as Fbs1 and forms an SCF-type ubiquitin ligase. The Fbs1 protein sequence shows highly homologous to that of Fbs2 other than the P domain of Fbs1 and C-terminal part of Fbs2, but the linker sequence between the F-box and FBA domains shows lower homology than other portions (Fig. 3*A*). As shown in Fig. 3*B*, the difference in the ability for assembling into the SCF complex between Fbs1 and Fbs2 is ascribed to the short linker sequence (92–117 amino acids of Fbs1). Although Fbs2 formed the SCF complex efficiently in the cytosol as well as the 100,000 × *g* precipitate fraction, the SCF^{Fbs1} formation was mainly present bound on the ER membrane (Fig. 3*C*). Although it is not clear whether the linker sequence of Fbs1 prevents the SCF^{Fbs1} from being in the cytosol or causes the formation of the SCF^{Fbs1} bound on the ER membrane, this limited localization of SCF^{Fbs1} is also due to the linker sequence (Fig. 3*C*). Crystal structure and mutational analyses of Cdc4 and βTrCP1 revealed the importance of orientation and rigidity in the linker sequence between F-box and WD40 domains for their *in vivo* function (23, 24). The linker sequences of Cdc4 and βTrCP1 are longer than that of Fbs1 and form three or four helix globular domains. On the other hand, the linker sequence of Fbs1 is an unstructured domain that consists of a flexible linker loop and an α-helix and is too far from Cul1 to influence directly the SCF complex formation.[3] The information of the structure of Skp1-Fbs1 suggests that the prevention of the SCF complex formation by this unstructured linker sequence can be cancelled by binding to the membrane or unidentified proteins on the ER.

In this study, we demonstrated that the Fbs1 could suppress the aggregation of denatured glycoproteins. This activity is due to the N-terminal P domain that is not seen in other F-box proteins. This N-terminal domain has been reported as a PEST sequence rich in proline, glutamic acid, serine, and threonine, which are often found in short-lived proteins (25). The N-terminal sequence in Fbs1, however, did not seem to act as a general PEST because the deletion of the P domain from Fbs1 or the addition to Fbs2 did not affect the protein stability (Fig. 3). More recently, it has been reported that U-box type E3 CHIP (C terminus of Hsc-70-interacting protein) is associated with Fbs1 through the P domain (26). Although we did not detect the E3 activity of the Skp1-Fbs1 dimers produced in the insect cells toward glycoprotein substrate GlcNAc-terminated fetuin (Fig. 5*B*), it is possible that an unknown chaperone molecule of insect cells was bound to the P domain of Fbs1. Skp1-Fbs1 dimers and Fbs1 monomers as well as the SCF^{Fbs1} complex showed activity to suppress the denatured glycoprotein aggregation, suggesting that the majority of Fbs1 is present as Skp1-Fbs1 dimers or Fbs1 monomers in cells and is not an intermediate prior to assembly of the SCF^{Fbs1} complex, but rather, a novel functional unit.

It is predicted that more than 30% of eukaryotic proteins contain substantial regions of disordered structure (27). One feature of intrinsically disordered proteins is their rapid degradation. Intracellular protein quality control, especially the degradation of proteins with aberrant structures, is thought to be important particularly in quiescent cells such as neurons (28). Fbs1 is expressed mainly in neuronal cells in the adult brain (14). Recently, it has been reported (29, 30) that loss of autophagy leads to neurodegeneration even in the absence of any

[3] Mizushima, T., Yoshida, Y., Kumanomidou, T., Hasegawa, Y., Suzuki, A., Yamane, T., and Tanaka, K., unpublished data.

aggregation-prone mutant proteins. Moreover, these reports have shown that the primary role of autophagy under normal conditions is the turnover of diffused cytosolic proteins, rather than direct elimination of inclusion bodies (29, 30). Our study suggests that Fbs1 contributes to the clearance of such cytosolic proteins by constitutive autophagy, like other chaperone systems, to suppress the aggregation of abnormal glycoproteins in neurons. For this, the N-terminal unique sequence of Fbs1, the P domain, having chaperone function, may have been made up during evolution. Since Cul1 is a common component of the SCF complexes and Fbs1 is abundant in neuronal cells, Fbs1 may also evolutionally acquire the linker sequence that suppresses the SCF^{Fbs1} complex formation to supply Cul1 toward other F-box proteins. It also seems possible that Fbs1 functions as a chaperone to keep the solubility of a particular glycoprotein(s) in the cytosol in neuronal cells. Further studies are needed to identify the Fbs1 target glycoproteins in neuronal cells, which may reveal the role of Fbs1 in maintaining homeostasis of neuronal cells.

Acknowledgment—We thank M. E. Cheetham for generously providing rhodopsin constructs.

REFERENCES

1. Feldman, R. M., Correll, C. C., Kaplan, K. B., and Deshaies, R. J. (1997) *Cell* **91,** 221–230
2. Skowyra, D., Craig, K. L., Tyers, M., Elledge, S. J., and Harper, J. W. (1997) *Cell* **91,** 209–219
3. Bai, C., Sen, P., Hofmann, K., Ma, L., Goebl, M., Harper, J. W., and Elledge, S. J. (1996) *Cell* **86,** 263–274
4. Jin, J., Cardozo, T., Lovering, R. C., Elledge, S. J., Pagano, M., and Harper, J. W. (2004) *Genes Dev.* **18,** 2573–2580
5. Ilyin, G. P., Serandour, A. L., Pigeon, C., Rialland, M., Glaise, D., and Guguen-Guillouzo, C. (2002) *Gene (Amst.)* **296,** 11–20
6. Winston, J. T., Koepp, D. M., Zhu, C., Elledge, S. J., and Harper, J. W. (1999) *Curr. Biol.* **9,** 1180–1182
7. Yoshida, Y., Tokunaga, F., Chiba, T., Iwai, K., Tanaka, K., and Tai, T. (2003) *J. Biol. Chem.* **278,** 43877–43884
8. Yoshida, Y., Chiba, T., Tokunaga, F., Kawasaki, H., Iwai, K., Suzuki, T., Ito, Y., Matsuoka, K., Yoshida, M., Tanaka, K., and Tai, T. (2002) *Nature* **418,** 438–442
9. Mizushima, T., Hirao, T., Yoshida, Y., Lee, S. J., Chiba, T., Iwai, K., Yamaguchi, Y., Kato, K., Tsukihara, T., and Tanaka, K. (2004) *Nat. Struct. Mol. Biol.* **11,** 365–370
10. Yoshida, Y. (2005) *Methods Enzymol.* **398,** 159–169
11. Yoshida, Y., Adachi, E., Fukiya, K., Iwai, K., and Tanaka, K. (2005) *EMBO Rep.* **6,** 239–244
12. Tanahashi, N., Murakami, Y., Minami, Y., Shimbara, N., Hendil, K. B., and Tanaka, K. (2000) *J. Biol. Chem.* **275,** 14336–14345
13. Paquet, M. E., Leach, M. R., and Williams, D. B. (2005) *Methods (Oxf.)* **35,** 338–347
14. Erhardt, J. A., Hynicka, W., DiBenedetto, A., Shen, N., Stone, N., Paulson, H., and Pittman, R. N. (1998) *J. Biol. Chem.* **273,** 35222–35227
15. Illing, M. E., Rajan, R. S., Bence, N. F., and Kopito, R. R. (2002) *J. Biol. Chem.* **277,** 34150–34160
16. Saliba, R. S., Munro, P. M., Luthert, P. J., and Cheetham, M. E. (2002) *J. Cell Sci.* **115,** 2907–2918
17. Stronge, V. S., Saito, Y., Ihara, Y., and Williams, D. B. (2001) *J. Biol. Chem.* **276,** 39779–39787
18. Cardozo, T., and Pagano, M. (2004) *Nat Rev. Mol. Cell. Biol.* **5,** 739–751
19. Petroski, M. D., and Deshaies, R. J. (2005) *Nat. Rev. Mol. Cell. Biol.* **6,** 9–20
20. Galan, J. M., Wiederkehr, A., Seol, J. H., Haguenauer-Tsapis, R., Deshaies, R. J., Riezman, H., and Peter, M. (2001) *Mol. Cell. Biol.* **21,** 3105–3117
21. Kaplan, K. B., Hyman, A. A., and Sorger, P. K. (1997) *Cell* **91,** 491–500
22. Russell, I. D., Grancell, A. S., and Sorger, P. K. (1999) *J. Cell Biol.* **145,** 933–950
23. Orlicky, S., Tang, X., Willems, A., Tyers, M., and Sicheri, F. (2003) *Cell* **112,** 243–256
24. Wu, G., Xu, G., Schulman, B. A., Jeffrey, P. D., Harper, J. W., and Pavletich, N. P. (2003) *Mol. Cell* **11,** 1445–1456
25. Rechsteiner, M., and Rogers, S. W. (1996) *Trends Biochem. Sci.* **21,** 267–271
26. Nelson, R. F., Glenn, K. A., Miller, V. M., Wen, H., and Paulson, H. L. (2006) *J. Biol. Chem.* **281,** 20242–20251
27. Fink, A. L. (2005) *Curr. Opin. Struct. Biol.* **15,** 35–41
28. Forman, M. S., Trojanowski, J. Q., and Lee, V. M. (2004) *Nat. Med.* **10,** 1055–1063
29. Hara, T., Nakamura, K., Matsui, M., Yamamoto, A., Nakahara, Y., Suzuki-Migishima, R., Yokoyama, M., Mishima, K., Saito, I., Okano, H., and Mizushima, N. (2006) *Nature* **441,** 885–889
30. Komatsu, M., Waguri, S., Chiba, T., Murata, S., Iwata, J., Tanida, I., Ueno, T., Koike, M., Uchiyama, Y., Kominami, E., and Tanaka, K. (2006) *Nature* **441,** 880–888

Structural basis for the selection of glycosylated substrates by SCF^{Fbs1} ubiquitin ligase

Tsunehiro Mizushima*†, Yukiko Yoshida‡, Taichi Kumanomidou*, Yuko Hasegawa*, Atsuo Suzuki*, Takashi Yamane*§, and Keiji Tanaka‡§

*Department of Biotechnology, Graduate School of Engineering, Nagoya University, Chikusa-ku, Nagoya 464-8603, Japan; †Precursory Research for Embryonic Science and Technology, Japan Science and Technology Agency, Kawaguchi, Saitama 332-0012, Japan; and ‡Laboratory of Frontier Science, Tokyo Metropolitan Institute of Medical Science, Bunkyo-ku, Tokyo 113-8613, Japan

Edited by John Kuriyan, University of California, Berkeley, CA, and approved February 21, 2007 (received for review November 21, 2006)

The ubiquitin ligase complex SCF^{Fbs1}, which contributes to the ubiquitination of glycoproteins, is involved in the endoplasmic reticulum-associated degradation pathway. In SCF ubiquitin ligases, a diverse array of F-box proteins confers substrate specificity. Fbs1/Fbx2, a member of the F-box protein family, recognizes high-mannose oligosaccharides. To elucidate the structural basis of SCF^{Fbs1} function, we determined the crystal structures of the Skp1–Fbs1 complex and the sugar-binding domain (SBD) of the Fbs1–glycoprotein complex. The mechanistic model indicated by the structures appears to be well conserved among the SCF ubiquitin ligases. The structure of the SBD–glycoprotein complex indicates that the SBD primarily recognizes $Man_3GlcNAc_2$, thereby explaining the broad activity of the enzyme against various glycoproteins. Comparison of two crystal structures of the Skp1–Fbs1 complex revealed the relative motion of a linker segment between the F-box and the SBD domains, which might underlie the ability of the complex to recognize different acceptor lysine residues for ubiquitination.

glycoprotein | tertiary structure | ubiquitin system

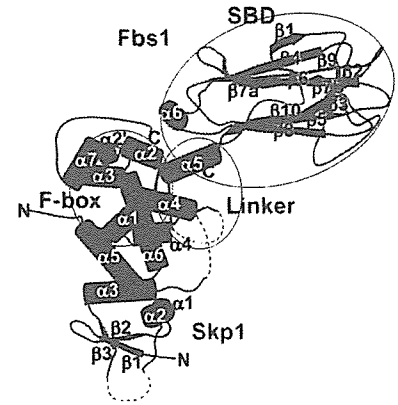

Fig. 1. Structure of the Skp1–Fbs1 complex. Skp1 and Fbs1 are colored blue and red, respectively. The secondary structure elements for Skp1 and Fbs1 are labeled. Dotted lines represent disordered regions. The F-box, linker, and SBD domains of Fbs1 are circled.

Ubiquitin-mediated proteolysis plays a regulatory role in a number of diverse cellular processes and involves the selective destruction of short-lived functional proteins (1). The ubiquitin–proteasome system also is responsible for the disposal of misfolded and unfolded cellular proteins, the aberrant accumulation of which usually causes cell death, which can lead to neurodegenerative diseases (2). Protein ubiquitination is catalyzed by a sophisticated cascade system consisting of the ubiquitin-activating (E1), ubiquitin-conjugating (E2), and ubiquitin-ligating (E3) enzymes (3). Among these enzymes, the E3 enzymes are responsible for the selection of target proteins. E3 enzymes are a diverse family of proteins and protein complexes. One of the best characterized groups of E3 enzymes is the SCF complex [composed of Skp1, Cul1, Rbx1 (also called Roc1), and an F-box protein], which regulates the degradation of a broad range of cellular proteins (4). F-box proteins consist of an N-terminal ≈40-aa F-box domain that binds to Skp1 and various C-terminal substrate-recognition regions and are subcategorized into three classes according to their substrate-binding domains. The Fbw (or FBXW) and Fbl (or FBXL) families possess WD40 repeats and leucine-rich repeats in their binding domains, respectively (5). The third class of F-box proteins is the Fbx (or FBXO) family, which does not contain any presumptive functional domains. However, we recently identified a subfamily within the Fbx family that consists of at least five homologous F-box proteins that recognize N-glycan; we named the sugar-binding domain (SBD)-containing proteins of this subfamily the Fbs (F-box protein that recognizes sugar chains; known previously as FBG) proteins (6).

In the SCF complex, Cul1 functions as a molecular scaffold that simultaneously interacts through its N and C termini with the crucial adaptor subunits Skp1 and Rbx1 together with a specific E2 enzyme, respectively. Skp1 is an adaptor protein that links Cul1 and one of the F-box proteins (6). Fbw and Fbl proteins usually recognize the phosphorylation status of the substrate, and structural models of the SCF complexes of some of these proteins, such as Fbw1/β-TrCP1 (7), Fbw7/Cdc4 (8), and Fbl1/Skp2 (9–11), have been reported. Structural information, however, is available only for the recognition of phosphorylated protein substrates.

N-linked glycosylation of proteins takes place in the endoplasmic reticulum and plays a key role in protein quality control (12). Misfolded proteins and unassembled protein complexes that fail to assume their functional states in the endoplasmic reticulum are subjected to endoplasmic reticulum-associated degradation, which involves retrotranslocation into the cytosol and degradation by the ubiquitin–proteasome system. SCF^{Fbs1} is an N-linked glycoprotein-specific ubiquitin ligase complex that contains the neuron-specific F-box protein Fbs1/Fbx2/NFB42 (13–16). We previously reported x-ray crystal structures of the Fbs1 SBD alone and in complex with di-*N*-acetylchitobiose (chitobiose, GlcNAc-GlcNAc, or $GlcNAc_2$), which revealed that the binding site is formed by a small hydrophobic pocket located at the top of a β-sandwich (17). The molecular mechanism

Author contributions: T.Y. and K.T. designed research; T.M., Y.Y., T.K., and Y.H. performed research; A.S. analyzed data; and T.M., Y.Y., and K.T. wrote the paper.

The authors declare no conflict of interest.

This article is a PNAS Direct Submission.

Abbreviations: RNaseB, ribonuclease B; SBD, sugar-binding domain.

Data deposition: The atomic coordinates and structure factors have been deposited in the Protein Data Bank, www.pdb.org (PDB ID codes 2E31, 2E32, and 2E33).

§To whom correspondence may be addressed. E-mail: yamane@nubio.nagoya-u.ac.jp or tanakak@rinshoken.or.jp.

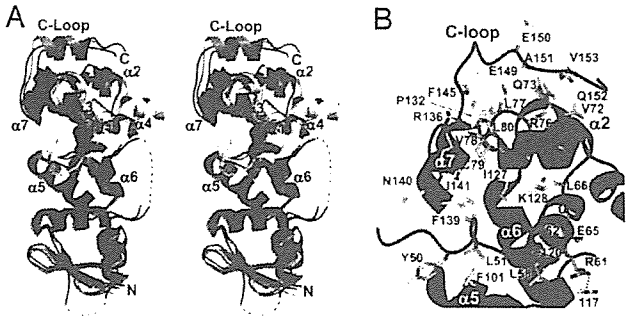

Fig. 2. Structure of the Skp1–Fbs1 interface. (*A*) Stereo views of the Fbs1 F-box domain (red) and Skp1 (blue) are compared with the structures of Skp1–Skp2 and Skp1–β-TrCP1. Skp1 is purple, Skp2 is green, Skp1 is orange, and β-TrCP1 is yellow. The secondary structure elements for Skp1 and Fbs1 are labeled with black and red letters, respectively. (*B*) Close-up view of the interface between Skp1 and Fbs1 showing intermolecular contacts. Fbs1 is red and Skp1 is blue.

underlying the ubiquitination of N-glycoproteins by the SCF^{Fbs1} ubiquitin ligase, however, is unknown at present. To understand the mechanistic details of the SCF^{Fbs1}-mediated ubiquitination reaction, we determined the crystal structures of the SBD–glycoprotein and Skp1–Fbs1 complexes.

Results

Overall Structure of the Skp1–Fbs1 Complex. The Skp1–Fbs1 complex has an overall L-shaped structure with Skp1 and the Fbs1 subunits oriented ≈90° to each other (Fig. 1). Skp1 and the chitobiose-binding site (17) are located at the opposite ends of Fbs1. Fbs1 consists of four distinct domains: the PEST domain (residues 1–54), the F-box domain (residues 55–95), a linker domain (residues 96–124), and the SBD (residues 125–297). The electron densities of the N-terminal PEST domain (residues 1–47) and part of the linker domain (residues 104–108) are not visible, suggesting that these regions are flexible. Although the Skp1–Fbs1 complex was crystallized in the presence of 30 mM chitobiose, the chitobiose molecule is not visible in this structure. The F-box domain comprises four α helices, which is the same structural motif observed in the Skp1-binding domains of Skp2 and β-TrCP1 (Fig. 2*A*). The SBD in the Skp1–Fbs1 complex is composed of a 10-stranded antiparallel β-sandwich, and it can be superposed on the previously reported structure of SBD alone with an average rms deviation of 0.39 Å for the C^{α} atoms, indicating that the structures are very similar. On the other hand, the C-terminal linker helix α5 assumes slightly different positions in the two structures because of crystal packing and the flexibility of the linker domain, which consists of α5 and a loop structure.

The Skp1 in the Skp1–Fbs1 complex adopts the same BTB/POZ fold (18) observed in previously reported structures of Skp1 (7–9). Interestingly, the C-terminal α-helix α8 of previously reported structures of Skp1 complexed with other F-box proteins is replaced with an extended structure (C loop: residues 146–155) (Fig. 2*A*). The differences in the secondary structure of Skp1 may reflect different roles of the protein. With the exception of the C-terminal loop, the overall structure of Skp1 is almost identical to those of the protein in the Skp1–Skp2 and Skp1–β-TrCP1 complexes (rms deviations for the C^{α} atoms: 1.8 and 2.1 Å, respectively).

Skp1–F-Box Interface. Whereas the F-box domain of Fbs1 contains the same four-helix (α1–α4) structure seen in the domains of

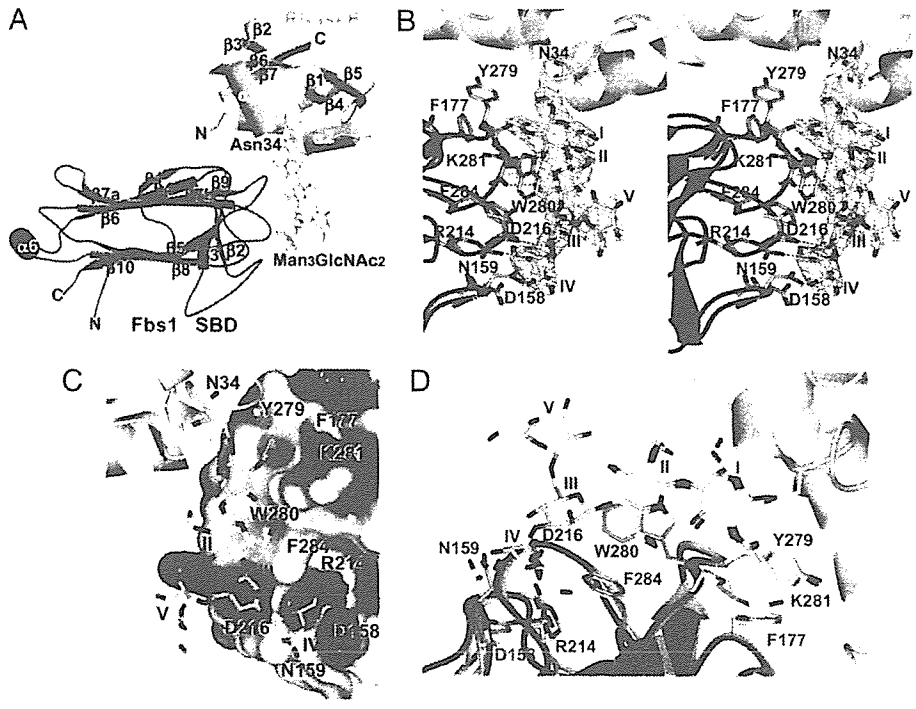

Fig. 3. Structure of the SBD–RNaseB complex. (*A*) The SBD is red and RNaseB is cyan. The secondary structure elements of the SBD and RNaseB are labeled. (*B*) Stereo view of the interface between the substrate-binding pocket of the SBD and the sugar of RNaseB. The $Man_3GlcNAc_2$ was modeled with the electron density map ($2F_o - F_c$ omit map of $Man_3GlcNAc_2$) contoured at 1.1 rms deviation. Fbs1 is red and RNaseB is cyan. (*C*) Surface representation of the substrate-binding pocket of the SBD bound to $Man_3GlcNAc_2$. The surface is colored according to the electrostatic potential of the residues (blue, positive; red, negative). (*D*) Comparison between the substrate-binding sites of the Fbs1 SBD (green) bound to chitobiose (yellow) and the Fbs1 SBD (red) bound to glycosylated RNaseB (cyan).

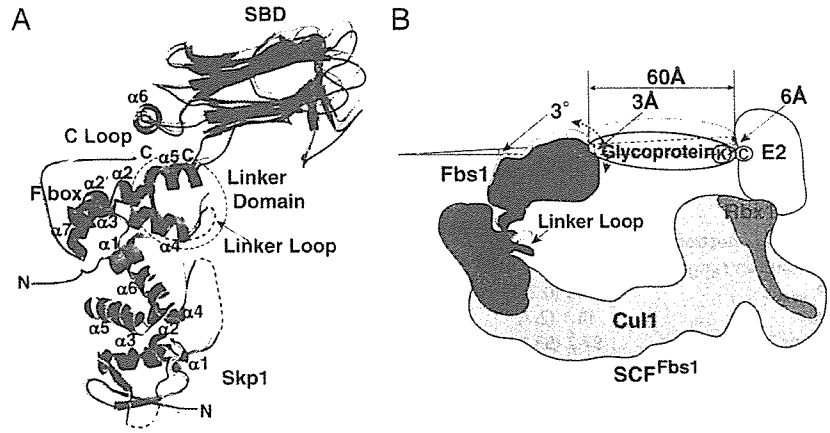

Fig. 4. Regulatory mechanism of SCF^{Fbs1} glycoprotein ubiquitination. (*A*) Comparison of the two crystal structures of the Skp1–Fbs1 complex. Skp1 (form 1), Fbs1 (form 1), Skp1 (form 2), and Fbs1 (form 2) are blue, red, yellow, and green, respectively. (*B*) Schematic representation of the model for ubiquitination on SCF^{Fbs1}. The E2 active-site cysteine and acceptor lysine residues are depicted with circled letters.

Skp2 (1.5-Å rms deviation for 27 C^{α} atoms) and β-TrCP1 (1.7-Å rms deviation for 28 C^{α} atoms), there are several differences. Helix α2 in Fbs1 is composed of two segments (α2 and α2′) separated by a turn, which causes it to bulge into the C loop of Skp1. The orientations of helices α3 and α4 of Fbs1 are similar to those of Skp2 but not to those of β-TrCP1 (Fig. 2*A*). Moreover, whereas the C-terminal region of the F-box domain of Skp2 is a loop structure, those of Fbs1 and β-TrCP1 form α-helices (α4).

The binding mode between Skp1 and the F-box domain of Fbs1 is almost identical to those between Skp1 and Skp2 (1.0-Å rms deviation for 120 C^{α} atoms) and between Skp1 and β-TrCP1 (1.1-Å rms deviation for 117 C^{α} atoms), except that the C loop of Skp1 interacts with the F-box domain through van der Waals contacts (Phe-145, Glu-149, Glu-150, Ala-151, Gln-152, and Val-153 of Skp1 interact with Val-72, Gln-73, Arg-76, Leu-77, and Leu-80 of Fbs1) (Fig. 2*B*). The positions of the Fbs1 F-box domain and α7 in Skp1 are shifted away from the N-terminal domain of Skp1 by ≈4.0 Å (Skp1–Skp2) or ≈2.5 Å (Skp1–β-TrCP1). These differences in the distances from the F-box domains to α7 of Skp1 and the C-terminal structures of Skp1 are likely due to the F-box structure.

Structure of the Glycoprotein Complex of the SBD. Ribonuclease B (RNaseB) is a glycoprotein that has a single high-mannose oligosaccharide ($Man_{6-8}GlcNAc_2$) attached at Asn-34 (19). RNaseB binds to the edge of the β-sandwich of the SBD (Fig. 3*A*). Clear electron density demonstrates the presence of $Man_3GlcNAc_2$ bound to the Fbs1 monomer, but the outer branches of the carbohydrate are disordered and not visible in the electron density map. The structure of the Fbs1-bound RNaseB, which consists of three α-helices and seven β-strands, is essentially identical to the previously reported structures of apo-RNaseB (20, 21); these structures have an average 0.59-Å rms deviation for the C^{α} positions. Similarly, the SBDs in the structures of the Skp1–Fbs1 and SBD–RNaseB complexes can be superposed with an average 0.48-Å rms deviation for the C^{α} positions, indicating that RNaseB binding does not cause any significant structural changes in the SBD.

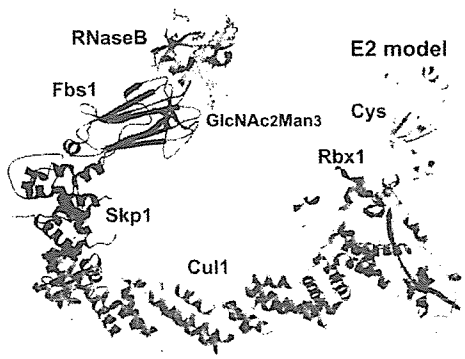

Fig. 5. Model of the SCF^{Fbs1}–RNaseB complex bound to E2. Cul1, Rbx1, Skp1, Fbs1, RNaseB, and E2 are green, orange, blue, red, cyan, and yellow, respectively. Lysine residues on the RNaseB surface are presented in ball-and-stick format and are coral.

Glycoprotein Recognition by the SBD in the SBD–RNaseB Complex. The sugar-binding surface consists of the four loops between β2 and β3, β3 and β4, β5 and β6, and β9 and β10. $Man_3GlcNAc_2$ interacts with nine Fbs1 residues (Asp-158, Asn-159, Phe-177, Arg-214, Asp-216, Tyr-279, Trp-280, Lys-281, and Phe-284) through hydrogen bonds and/or van der Waals contacts (Fig. 3 *B* and *C*). The molecular recognition mechanism between the chitobiose moiety and the amino acid residues in Fbs1 is similar to that reported previously for the SBD–chitobiose complex (17). The methyl group of the *N*-acetyl moiety from the GlcNAc (I) residue is inserted into a small hydrophobic pocket surrounded by the side chains of Phe-177, Tyr-279, and Lys-281; and the O3 atom forms a hydrogen bond with the main chain N atom of Lys-281. The GlcNAc (II) residue is stacked on the aromatic ring of Trp-280 and the O6 atom forms a hydrogen bond with the carbonyl oxygen atom of Lys-281. The two GlcNAc residues form an intramolecular hydrogen bond between the O3 atom of GlcNAc (I) and the O6 atom of GlcNAc (II). Formation of these hydrogen bonds fixes the orientation of the β(1→4)-linked GlcNAc residues. Comparison of the SBD–RNaseB complex and the previously reported SBD–chitobiose complex reveals that the substrate binding pockets (Phe-177, Tyr-279, Trp-280, and Lys-281) and the chitobiose structures can be superposed with an average rms deviation of 0.69 Å for all of the atoms (Fig. 3*D*). Only the side chain of Lys-281 has a different conformation, and it has been shown that Lys-281 is not essential for the binding to chitobiose (17). The outer mannose-binding residues of the SBD also do not exhibit significant conformational changes. We have reported that Fbs1 recognizes not only chitobiose but also the outer mannose branches (17). The O4 atom of Man(III)

BIOCHEMISTRY

Table 1. Data collection, phasing, and refinement statistics

	Skp1–Fbs1	Skp1–Fbs1/Thimerosal	Skp1–Fbs1	SBD–RNaseB
Data collection				
Space group	$P3_221$	$P3_221$	$P2_12_12_1$	$P432$
Cell parameters, Å				
a	106.7	106.6	66.2	148.6
b	106.7	106.6	111.1	148.6
c	110.2	113.7	153.3	148.6
Unique reflections	27,964	17,765	12,269	15,839
Resolution range, Å	2.40 (2.49–2.40)	2.80 (2.90–2.80)	3.50 (3.63–3.50)	2.70 (2.80–2.70)
R_{merge}	0.045 (0.327)	0.058 (0.328)	0.103 (0.225)	0.078 (0.325)
$I/\sigma I$	18.1 (2.7)	16.0 (2.2)	7.0 (4.1)	13.9 (5.2)
Completeness, %	97.7 (93.0)	95.7 (79.6)	85.2 (79.0)	99.4 (97.9)
Redundancy	5.4 (2.9)	6.2 (2.3)	2.6 (2.1)	11.8 (6.4)
Refinement				
No. of reflections	26,521		12,279	15,049
R_{work}/R_{free}	0.233/0.291		0.223/0.299	0.216/0.288
rms deviations				
Bond lengths, Å	0.010		0.022	0.026
Bond angles, °	1.33		2.08	2.51

Values in parentheses represent the highest-resolution shell.

forms a hydrogen bond with the sidechain O^{δ} atom of the Asp-216 sidechain; this hydrogen bond stabilizes the complex with the Manβ(1→4)GlcNAc$_2$ moiety. Clear electron density is observed between the β(1→4)-linked Man residue and Asp-216 in Fbs1. Furthermore, Asp-216 is conserved in other F-box proteins that contain an F-box-associated domain, suggesting that it plays a role in the recognition of oligosaccharides. Man(IV) forms hydrogen bonds with the sidechain N^{δ} atom of Asn-159 through the O2 atom and with the sidechain N^{η} atom of Arg-214 through the O5 atom. On the other hand, Man(V) protrudes from the binding site and does not interact with Fbs1. These results indicate that the GlcNAc$_2$ core, β(1→4)-linked Man(III), and α(1→3)-linked Man(IV) play significant roles in the binding to Fbs1. Whereas Man$_8$GlcNAc$_2$ is thought to be the major N-glycan among unfolded glycoproteins that are translocated into the cytosol for endoplasmic reticulum-associated degradation, our results indicate that Man$_3$GlcNAc$_2$ can be sufficiently recognized by the SCF^{Fbs1} complex. Indeed, various synthetic oligosaccharides were used to show that Man$_3$GlcNAc$_2$ and Man$_8$GlcNAc$_2$ have similar affinities for Fbs1 (22). On the other hand, the binding affinities of Man$_8$GlcNAc$_1$ and chitobiose for Fbs1 are several orders of magnitude lower than those of Man$_3$GlcNAc$_2$ and Man$_8$GlcNAc$_2$, indicating that Man$_3$GlcNAc$_2$ is required for efficient binding to Fbs1 (15, 22). Moreover, the binding site provides substrate selectivity and specificity based on its shape and hydrogen-bonding network.

There are limited contacts between the SBD and RNaseB; the interface involves only 514 Å^2 of surface-accessible area. The surface areas occupied by Man$_3$GlcNAc$_2$ and the protein portion of the substrate are 349 and 165 Å^2, respectively. In addition to the smaller contact area, the protein portion of RNaseB does not form a hydrogen bond with Fbs1, suggesting that Man$_3$GlcNAc$_2$, but not the protein in RNaseB, defines the interaction with Fbs1.

Linker Flexibility Might Accommodate a Range of Substrates. Two crystal forms were identified for Skp1–Fbs1 ($P3_221$ and $P2_12_12_1$ define form 1 and form 2, respectively). These two forms have essentially the same overall structure (rms deviation of 1.1 Å for the C^{α} atoms) (Fig. 4*A*). Whereas the Skp1 proteins are well aligned with each other, the SBD of Fbs1 in form 2 is tilted farther away from Skp1 by ≈3°. The 3° tilt angle of the SBD creates a 3-Å gap at the substrate-binding site and a 6-Å shift at the E2 active site. This flexibility seems to be due in part to the linker-domain structure of Fbs1 (Fig. 4*A*). Residues 100–103 and 113–115 are shifted significantly compared with form 1. Although the linkage between the F-box and WD40 domains does not seem to be exceedingly rigid in the yeast Cdc4 structure, deletion of helix α5 or the lengthening of helix α6 due to an insertion of amino acid residues disrupts Cdc4 function *in vivo*, suggesting that the orientation and rigidity of the linkage between the F-box and the substrate-binding domains is important for SCF function (8). In the structure of Fbs1, the interaction between α5 and the linker loop through van der Waals contacts (His-113 of the linker loop to Gln-115, Phe-119, and Arg-123 of α5) is not rigid, and residues 104–108 of the linker domain are not visible in the electron density map. This structure indicates that the linkage between the F-box domain and the SBD of Fbs1 is somewhat flexible. This feature might allow the protein to accommodate a range of substrates (Fig. 4*B*).

Discussion

In this study, we determined the crystal structures of two crystal forms of the Skp1–Fbs1 complex and the SBD–RNaseB complex at 2.4-, 3.5-, and 2.7-Å resolutions, respectively. The structure of the Skp1–Fbs1 complex illustrates a different class of F-box proteins within the SCF ubiquitin ligase model. A model of the SCF^{Fbs1}–RNaseB–E2 complex was generated simply by superposition of the Skp1 subunits from the Skp1–Fbs1 and Skp1–Cul1–Rbx1 structures (PDB ID code 1LDK), the RING-finger domains derived from Rbx1 and from the c-Cbl subunit of the c-Cbl-UbcH7 structure (PDB ID code 1FBV) (23), the E2 subunits of the c-Cbl-UbcH7 structure, and the SBD-RNaseB structure. In this SCF^{Fbs1}-RNaseB model, RNaseB points toward the E2-binding site on Rbx1 (Fig. 5). The distance between the E2 active-site cysteine and the substrate-binding site is ≈60 Å, which is similar to the value that was reported previously (7, 8, 10). Despite differences in the sizes of the substrates and the positions of ubiquitinated lysine residues, the distance between the E2 active-site cysteine and the substrate-binding site is conserved among the SCF complexes. The same mechanism that allows the E2 active-site cysteine to reach the ubiquitinated lysine residues of the substrates is used independently of the type of F-box protein.

In the case of RNaseB, the distances between the E2 active-site cysteine and the lysine residues in RNaseB are 58.6–88.4 Å in the model of the SCF^{Fbs1}–RNaseB–E2 complex, whereas the

lysine residues in RNaseB are between 5.3 and 36.9 Å away from Asn-34. RNaseB is smaller than the minimum distance required to reach E2. Actually, SCF^{Fbs1} was not able to ubiquitinate RNaseB *in vitro*. This could be because RNaseB is too small, the lysine residues are at the wrong positions, or RNaseB is fixed because of contacts between $Man_3GlcNAc_2$ and Fbs1.

One of the most important properties for ubiquitination is the rigidity of the SCF–ubiquitin–ligase complex structure, because it serves to correctly position the target protein and E2. The two crystal structures of the Skp1–Fbs1 complex described in the present study, however, show differences in the orientation of the SBD. We propose that SCF^{Fbs1} has the ability to nonspecifically ubiquitinate glycoproteins targeted to the endoplasmic reticulum-associated degradation pathway. The protein portion of a target glycoprotein bound to Fbs1 may rotate at the linkage site between the innermost GlcNAc moiety and the asparagine residue, and the acceptor lysine residue can be located at a variety of positions. In SCF^{Fbs1}, the relative motion of the linker domain between the F-box domain and the SBD might be necessary to accommodate the different positions of the acceptor lysine residues in the various endoplasmic reticulum-associated degradation substrates.

SCF^{Fbs1} is a functionally unique molecule that recognizes the innermost $Man_3GlcNAc_2$ in N-glycans as a marker of denatured proteins. Our results provide a mechanistic basis for the recognition and ubiquitination of various glycoproteins by SCF^{Fbs1}.

Materials and Methods

Protein Expression and Purification. The Skp1–Fbs1 complex was coexpressed from the pET28b plasmid (Novagen, Madison, WI) in BL21 (DE3) cells. Full-length Skp1 was expressed as a 6× His-tagged protein, and full-length Fbs1 was expressed as an untagged protein. The complex was purified stepwise by Ni affinity, anion exchange, and gel-filtration chromatography. The Skp1–Fbs1 complex was then concentrated to ≈10 mg/ml by ultrafiltration in 25 mM Tris·HCl (pH 7.5) and 1 mM DTT.

For the SBD–RNaseB complex (with SBD residues 105–297 of Fbs1), the SBD and RNaseB (Sigma, St. Louis, MO) were combined in a 1:1 molar ratio and purified by gel-filtration chromatography. Fractions containing the SBD–RNaseB complex were then concentrated to ≈10 mg/ml and used for crystallization.

Crystallization and Data Collection. Crystals of Skp1–Fbs1 and SBD–RNaseB were obtained at 20°C by using the sitting-drop vapor diffusion method. Skp1–Fbs1 crystals were grown from 2.0 M ammonium sulfate, 0.1 M sodium citrate (pH 5.7), and 30 mM chitobiose, which produced two crystal forms. The SBD–RNaseB crystals were prepared by using 2.0% (vol/vol) PEG 400, 0.1 M Hepes (pH 7.5), and 2.1 M ammonium sulfate.

Diffraction data sets for Skp1–Fbs1 and SBD–RNaseB were collected at beamline BL44XU (SPring-8, Hyogo, Japan). Data processing and reduction were carried out with the HKL program suite (24). The two crystal forms of Skp1–Fbs1 and the SBD–RNaseB crystals belong to the $P3_221$ (Skp1–Fbs1 form 1), $P2_12_12_1$ (Skp1–Fbs1 form 2), and $P432$ (SBD–RNaseB) space groups. Heavy-atom soaks of the Skp1–Fbs1 crystals (form 1) were performed in crystallization buffer with 1 mM thimerosal for 5 min. Data collection, phasing, and refinement statistics are summarized in Table 1.

Structure Determination and Refinement. The structure of Skp1–Fbs1 was determined by a combination of molecular replacement, single isomorphous replacement, and anomalous scattering with an Hg derivative. The initial single isomorphous replacement and anomalous scattering phases were calculated with SHARP (25) and then improved by density modification with DM (26). Molecular replacement with the program MOLREP (27) was used to locate the Skp1 and SBD portions of the complex with search models consisting of Skp1 from SCF (PDB ID code 1LDK) and the SBD of Fbs1 (PDB ID code 1UMH). The model was further built with the program COOT (28) and then was improved by several cycles of manual rebuilding and refinement with the program REFMAC5 (29). The structure of crystal form 2 was solved by molecular replacement using MOLREP with the refined model of form 1.

The structure of SBD–RNaseB was determined by using the molecular replacement technique, MOLREP, and the structures of the SBD and RNaseB. The refined model contains residues 123–297 of the SBD and residues 1–124 of RNaseB. Phasing and refinement statistics are summarized in Table 1. There are no residues in disallowed regions of the Ramachandran plot. Structure figures were generated by using MOLSCRIPT (30), RASTER3D (31), and CCP4MG (32).

We thank Tomitake Tsukihara for helpful advice and stimulating discussions at all stages of the x-ray crystallographic analysis and the members of beamline BL44XU for help during the data collection at SPring-8. This work was supported in part by Grant-in-Aid for Scientific Research in Priority Areas 18054011 from the Ministry of Education, Culture, Sports, Science, and Technology (Japan).

1. Hershko A, Ciechanover A, Varshavsky A (2000) *Nat Med* 6:1073–1081.
2. Sherman MY, Goldberg AL (2001) *Neuron* 29:15–32.
3. Pickart CM (2001) *Annu Rev Biochem* 70:503–533.
4. Deshaies RJ (1999) *Annu Rev Cell Dev Biol* 15:435–467.
5. Jin J, Cardozo T, Lovering RC, Elledge SJ, Pagano M, Harper JW (2004) *Genes Dev* 18:2573–2580.
6. Yoshida Y (2003) *J Biochem (Tokyo)* 134:183–190.
7. Wu G, Xu G, Schulman BA, Jeffrey PD, Harper JW, Pavletich NP (2003) *Mol Cell* 11:1445–1456.
8. Orlicky S, Tang X, Willems A, Tyers M, Sicheri F (2003) *Cell* 112:243–256.
9. Schulman BA, Carrano AC, Jeffrey PD, Bowen Z, Kinnucan ER, Finnin MS, Elledge SJ, Harper JW, Pagano M, Pavletich NP (2000) *Nature* 408:381–386.
10. Zheng N, Schulman BA, Song L, Miller JJ, Jeffrey PD, Wang P, Chu C, Koepp DM, Elledge SJ, Pagano M, *et al.* (2002) *Nature* 416:703–709.
11. Hao B, Zheng N, Schulman BA, Wu G, Miller JJ, Pagano M, Pavletich NP (2005) *Mol Cell* 20:9–19.
12. Ellgaard L, Helenius A (2003) *Nat Rev Mol Cell Biol* 4:181–191.
13. Erhardt JA, Hynicka W, DiBenedetto A, Shen N, Stone N, Paulson H, Pittman RN (1998) *J Biol Chem* 273:35222–35227.
14. Yoshida Y, Chiba T, Tokunaga F, Kawasaki H, Iwai K, Suzuki T, Ito Y, Matsuoka K, Yoshida M, Tanaka K, *et al.* (2002) *Nature* 418:438–442.
15. Yoshida Y, Tokunaga F, Chiba T, Iwai K, Tanaka K, Tai T (2003) *J Biol Chem* 278:43877–43884.
16. Yoshida Y, Adachi E, Fukiya K, Iwai K, Tanaka K (2005) *EMBO Rep* 6:239–244.
17. Mizushima T, Hirao T, Yoshida Y, Lee SJ, Chiba T, Iwai K, Yamaguchi Y, Kato K, Tsukihara T, Tanaka K (2004) *Nat Struct Mol Biol* 11:365–370.
18. Aravind L, Koonin EV (1999) *J Mol Biol* 285:1353–1361.
19. Liang CJ, Yamashita K, Kobata A (1980) *J Biochem (Tokyo)* 88:51–58.
20. Williams RL, Greene SM, McPherson A (1987) *J Biol Chem* 262:16020–16031.
21. Ko TP, Williams R, McPherson A (1996) *Acta Crystallogr D* 52:160–164.
22. Hagihara S, Totani K, Matsuo I, Ito Y (2005) *J Med Chem* 48:3126–3129.
23. Zheng N, Wang P, Jeffrey PD, Pavletich NP (2000) *Cell* 102:533–539.
24. Otwinowski Z, Minor W (1997) *Methods Enzymol* 276:307–326.
25. Bricogne G, Vonrhein C, Flensburg C, Schiltz M, Paciorek W (2003) *Acta Crystallogr D* 59:2023–2030.
26. Collaborative Computational Project 4 (1994) *Acta Crystallogr D* 50:760–763.
27. Vagin AA, Teplyakov A (1997) *J Appl Crystallogr* 30:1022–1025.
28. Emsley P, Cowtan K (2004) *Acta Crystallogr D* 60:2126–2132.
29. Murshudov GN, Vagin AA, Dodson EJ (1997) *Acta Crystallogr D* 53:240–255.
30. Kraulis PJ (1991) *J Appl Crystallogr* 24:946–950.
31. Merritt EA, Murphy ME (1994) *Acta Crystallogr D* 50:869–873.
32. Potterton E, McNicholas S, Krissinel E, Cowtan K, Noble M (2002) *Acta Crystallogr D* 58:1955–1957.

Cell Death and Differentiation (2007), 1–8

www.nature.com/cdd

Review

Constitutive autophagy: vital role in clearance of unfavorable proteins in neurons

M Komatsu[1,2,3], T Ueno[1], S Waguri[4], Y Uchiyama[5], E Kominami[1] and K Tanaka*[,2]

Investigations pursued during the last decade on neurodegenerative diseases have revealed a common mechanism underlying the development of such diseases: conformational disorder of certain proteins leads to the formation of misfolded protein oligomers, which subsequently develop into large protein aggregates. These aggregates entangle other denatured proteins and lipids to form disease-specific inclusion bodies. The failure of the ubiquitin-proteasome system to shred the protein aggregates has led investigators to focus their attention to autophagy, a bulk degradative system coupled with lysosomes, which is involved in non-selective shredding of large amounts of cytoplasmic components. Research in this field has demonstrated the accumulation of autophagic vacuoles and intracytoplasmic protein aggregates in patients with various neurodegenerative diseases. Although autophagy fails to degrade large protein aggregates once they are formed in the cytoplasm, drug-induced activation of autophagy is effective in preventing aggregate deposition, indicating that autophagy significantly contributes to the clearance of aggregate-prone proteins. The pivotal role of autophagy in the clearance of aggregate-prone proteins has been confirmed by a deductive approach using a brain-specific autophagy-ablated mouse model. In this review, we discuss the consequences of autophagy deficiency in neurons.
Cell Death and Differentiation advance online publication, 2 March 2007; doi:10.1038/sj.cdd.4402120

Cell proteins exist in a balance between continuous synthesis and degradation. In general, this flow of synthesis and degradation (i.e., turnover) contributes to exertion of cell-type-specific functions and maintenance of cell homeostasis. However, it is not uncommon that living cells are exposed to various environmental stresses, such as oxygen radicals and UV irradiation. Unfortunately, these stresses frequently cause various types of protein injuries that vitiate normal cellular functions or homeostasis and may eventually cause cell death. Prompt elimination of injured harmful proteins, which is particularly important in non-proliferative cells, such as neurons, is totally dependent on proper function of protein catabolic machineries, in which two major sophisticated apparatuses play principal roles. One is the proteasome, which is an elegantly organized multi-protease complex with catalytic activities inside its central proteinaceous chamber. It plays crucial roles in selective degradation of short-lived regulatory proteins as well as proteins with aberrant structures that should be eliminated from the cells.[1] The other apparatus is the lysosome that contains many acidic hydrolases, which are separated from the cytosol by the limiting membrane. In this lysosomal pathway, degradation of plasma membrane proteins and extracellular proteins is mediated by endocytosis, whereas that of cytoplasmic components is achieved through distinct types of autophagic pathways; for example, macroautophagy, microautophagy, and chaperone-mediated autophagy.[2,3]

Macroautophagy (hereafter referred to as autophagy), the major type of autophagy, is the bulk protein degradation pathway associated with marked membrane dynamics. In response to various stimuli, such as starvation (i.e., nutritional step-down) and humoral (trophic) factors (e.g., glucagon and cytokines), an isolation membrane appears promptly in the cytosol, where it gradually elongates to sequestrate cytoplasmic constituents. Subsequently, the edges of the membrane fuse together to form double-membrane structures termed autophagosomes. Autophagosomes rapidly fuse with lysosomes, and their contents engulfed together with the inner membrane are degraded by a variety of lysosomal digestive hydrolases (Figure 1).[4] In addition to the importance of starvation-induced (i.e., adaptive) autophagy equipped as a fundamental survival strategy in all eukaryotic cells, growing lines of evidence point to the importance of basal autophagy that operates constitutively at low rate even under nutrient-rich environment and to its key role in global turnover of cellular components including organelles.

[1]Department of Biochemistry, Juntendo University School of Medicine, Tokyo, Japan; [2]Laboratory of Frontier Science, Tokyo Metropolitan Institute of Medical Science, Tokyo, Japan; [3]PRESTO, Japan Science and Technology Corporation, Kawaguchi, Japan; [4]Department of Anatomy and Histology, Fukushima Medical University School of Medicine, Fukushima, Japan and [5]Department of Cell Biology and Neurosciences, Osaka University Graduate School of Medicine, Osaka, Japan
*Corresponding author: K Tanaka, Laboratory of Frontier Science, Tokyo Metropolitan Institute of Medical Science, Bunkyo-ku, Tokyo 113-8613, Japan.
Tel/Fax: +81 3 3823 2237; E-mail: tanakak@rinshoken.or.jp
Keywords: autophagy; neurodegenerative diseases; ubiquitin; knockout-mice; Atg7
Abbreviations: AD, Alzheimer's disease; APP, amyloid precursor protein; Aβ, beta-amyloid; GFP, green fluorescent protein; HD, Huntington's disease; LC3, microtubule-associated protein 1 light chain 3/MAP1LC3; mTor, mammalian target of rapamycin; PD, Parkinson's disease; PS1, presenilin-1; SDH, succinate dehydrogenase; TCA, tricarboxylic acid
Received 28.11.06; revised 05.2.07; accepted 05.2.07; Edited by E Baehrecke

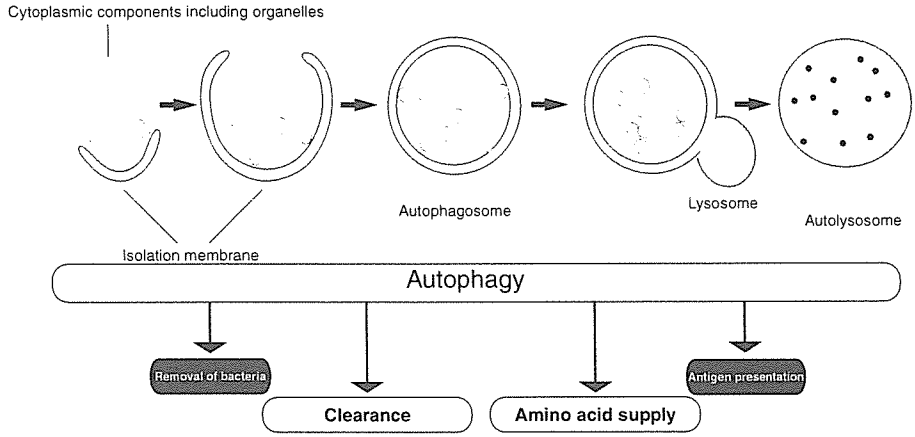

Figure 1 Schematic representation of the physiological functions of autophagy. Autophagy is induced in response to emergency states such as nutrient starvation or bacterial infection, which results in the degradation of cytoplasmic components for amino-acid supply (non-selective process) and the removal of bacteria that invade the cytoplasm (selective process). Autophagy also contributes to processing viral proteins such as EBNA1 and certain cytosolic proteins (e.g., tumor antigens) for presentation onto major histocompatibility complex (MHC) class II molecules. Autophagy also occurs constitutively even under a nutrient-rich state and contributes to global turnover of cellular components. It is an essential cellular process that maintains homeostasis in quiescent cells (e.g., hepatocytes and neurons)

Starvation-induced Autophagy

The most fundamental function of autophagy is cellular adaptation to nutritional stress. In yeast, autophagy is promptly induced upon nitrogen starvation.[5] Transgenic mice overexpressing GFP (green fluorescent protein)-LC3 is an interesting animal model for monitoring autophagy.[6] LC3 (microtubule-associated protein 1 light chain 3/MAP1LC3), originally identified as a small subunit of MAP-1A/MAP-1B, is processed by Atg4B protease to expose the carboxyl-terminal glycine whose residue serves as a donor site for conjugation of target molecules.[7–9] The processed form (LC3-I) undergoes two consecutive ubiquitylation-like modification reactions catalyzed by Atg7 (E1, activating-like enzyme) and Atg3 (E2, conjugating-like enzyme), to be covalently coupled with phosphatidylethanolamine (PE).[10–12] The PE-conjugated form, designated as LC3-II, is then recruited to autophagosomal membrane. Thus, LC3-II is a promising marker for autophagosomal membranes.[7] Similar to endogenous LC3, GFP-LC3 responds to nutrient-starved conditions to form GFP-LC3-II, which is recruited to autophagosomes in GFP-LC3 transgenic mice.[6] The autophagosomal GFP-LC3-II could be detected as dots in fluorescence microscopic analyses. Under fasting conditions, the numbers of fluorescent dots increase in the cytoplasm of the liver, heart, and skeletal muscles of GFP-LC3 transgenic mice.

Starvation-induced protein degradation has been best investigated in the liver. One unequivocal characteristic of hepatic protein degradation is its dependence on the nutrient conditions. Depending on the dietary cycle of the animal, the rate of protein degradation fluctuates between ~1.5% (fed state) and ~4.5% (fasted state) of total liver proteins per hour.[13] Recently, we generated *Atg7*$^{F/F}$:Mx1 mice in which autophagy could be successfully inactivated in the livers.[14] Whereas the amount of total liver proteins decreased to about 66% in the control liver by 1-day fasting, fasting did not result in a significant decrease in the amount of total proteins in the autophagy-deficient liver, indicating that the decrease in total proteins upon fasting is indeed dependent on autophagy. Measurement of the activity of mitochondrial enzyme, succinate dehydrogenase (SDH), showed that fasting was also associated with a significant decrease in SDH activity in total extracts in the control livers, and such reduction was proportional with the decrease in the amount of total protein. On the other hand, fasting was not associated with any change in SDH activity in the autophagy-deficient livers. These results suggest that the mitochondria and cytoplasmic proteins are proportionally degraded upon fasting by autophagy. Thus, it is plausible that autophagosomes surround cytoplasmic components including mitochondria at random to adapt for starvation.

Yeast deficient in autophagy rapidly dies under nutrition-poor conditions,[15] suggesting the important roles of autophagy in maintaining nutrient supply. Indeed, newborn mice deficient in Atg5 or Atg7, which are indispensable for autophagosome formation, show poor response to starvation with regard to production of amino acids, and die within the first day of life.[14,16] Furthermore, Lum *et al.*[17] reported that in IL-3-dependent cells, which cannot undergo apoptosis due to knockout of both Bax and Bak, impairment of autophagy leads to rapid cell death by loss of IL-3, and such death is suppressed by addition of methylpyruvate, a TCA (tricarboxylic acid) substrate. These results suggest that one of the important roles of autophagy is the supply of amino acids under nutrient-poor environment (Figure 2, top panel).

Unique Features of Neuronal Autophagy

The brain appears to be a specially protected tissue where nutrients (e.g., amino acids, glucose, and ketone bodies) are compensated by constant supply from other organs even under starvation conditions and consequently autophagy does not operate in response to nutritional stress. Indeed, autophagosomes-related GFP-LC3 dots do not increase at all

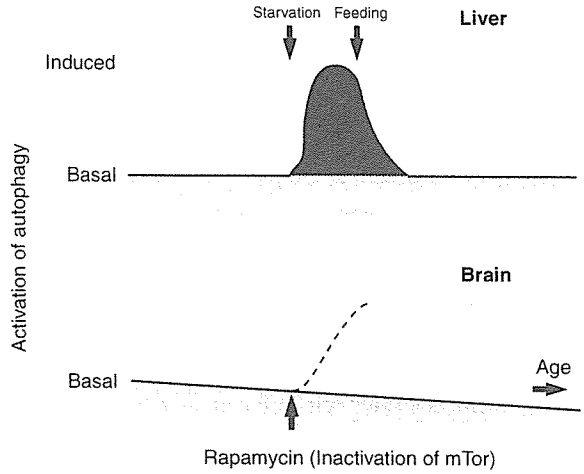

Figure 2 Schematic presentation of induced autophagy and basal (constitutive) autophagy. Under nutrient-rich conditions, autophagic proteolysis proceeds in hepatocytes at a basal rate (top panel, pink zone), which is enhanced two- to threefold to an induced rate under nutrient-starvation conditions (blue zone). When animals are re-fed, the rate of autophagic proteolysis promptly returns to the basal level. In contrast to the liver, autophagy in the brain is thought to proceed at a basal rate, irrespective of nutrient conditions. However, this basal or constitutive autophagy plays a critical role in the quality control system of neurons. Rapamycin and its homologs, which upregulate autophagy to an induced level (bottom panel, broken line), are expected to prevent the accumulation of aggregate-prone proteins. It should be noted that autophagic activity declines with age, which may relate to the age-dependent onset of neurodegenerative diseases

in the brain of GFP-LC3 transgenic mice, irrespective of fasting.[6] A reasonable conclusion drawn from these observations is that autophagy in the brain proceeds at a basal rate but is not enhanced under fasting conditions (Figure 2, bottom panel). Another peculiar feature of autophagy in neurons is the free localization of autophagosomes in the cytoplasm but the restriction of lysosomes mainly to the juxtanuclear cytoplasm of the cell body in the neuron. This feature means that autophagosomes formed in dendrites and synaptic terminal regions must be transported to the lysosome in the cell body. A previous kinetic analysis of organelle movements in cultured neurons indicated that phase-dense vesicles, containing sequestered cytoplasmic proteins and materials taken up by endocytosis, move along microtubules in the axon to the lysosomes in the cell body.[18] These data suggest that fusion of autophagosomes formed in the synaptic cytoplasm with lysosomes is strictly dependent on retrograde axonal transport. It has been reported that mutations of dynein and dynactin in mice and human cause motor neuron degeneration resembling amyotrophic lateral sclerosis.[19,20] Using cultured PC12 cells, flies and mice expressing different kinds of aggregate-prone proteins, such as expanded polyQ and mutant α-synuclein, Ravikumar *et al.*[21] demonstrated that inhibition of dynein function retarded the clearance of aggregates by inhibiting autophagosome-lysosome fusion. It has been shown recently that aggregate-prone proteins formed in the cytoplasm of cultured HeLa cells and a cultured neural cell line, are degraded by autophagy, which is also dependent on intact microtubules.[22]

Autophagic Vacuoles in Neurodegenerative Diseases

Morphological analyses revealed that accumulation of abnormally large number of autophagic vacuoles (autophagosomes plus autolysosomes) or the appearance of irregularly shaped autophagic vacuoles is frequently observed as a common feature in many inherited neurodegenerative diseases.[23–27] Inclusion bodies, composed of ubiquitin-positive cytoplasmic remnants, and lipofuscin deposits, together with dispersed autophagic vacuoles and lysosomes are the primary hallmarks of the late stages of these diseases. Increased density of autophagic vacuoles seems to reflect enhanced autophagosome formation, on one hand, but their accumulation with blurred structures of sequestered materials in their lumen may also imply impaired autolysosomal degradation, on the other. In fact, these morphological features are not present in normal neurons and resemble those of cultured HEK293 cells that have been placed under starvation conditions in the presence of lysosomal proteinase inhibitors.[28] Under these conditions, autophagic response is markedly enhanced, but autophagic proteolysis is simultaneously inhibited. In addition, as observed in Danon disease, which is caused by mutation of the lysosome-associated membrane protein-2 (LAMP-2), and LAMP-2-deficient mice, impairment of autophagosome-lysosome fusion also leads to unequivocal increment of autophagosomes in cardiac muscles and hepatocytes.[29,30]

Autophagy in Alzheimer's, Huntington's, and Parkinson's Diseases

Protein conformational disorders, such as Alzheimer's disease (AD), Huntington's disease (HD), and Parkinson's disease (PD), are characterized by abnormally high accumulation of misfolded and/or unfolded proteins in the surviving neurons as detected at postmortem examination. In this section, we will evaluate the role of autophagy in those hereditary neurodegenerative diseases.

It has become clear that autophagy is linked to the pathogenesis of HD. HD is an autosomal dominant disorder caused by mutations of huntingtin, a cytosolic protein that has a polyglutamine (polyQ) tract in its N-terminus. In HD, abnormal expansion of polyQ caused by codon (CAG) reiterations in exon 1 of the Huntingtin gene produces mutated huntingtin with an expanded polyQ repeat (more than 37 polyQs). Mutant huntingtin with a longer polyQ tract has a stronger tendency than the wild type to form aggregates, both accelerating the onset and worsening the severity of the disease, suggesting that the progressive formation of insoluble polyQ aggregates is a key event leading to manifestation of the disease. Indeed, model mouse with mutant polyQ is associated with formation of nuclear and cytoplasmic inclusions in their neurons.[31] However, recent studies revealed that globular and protofibrillar intermediates form before the organization of mature huntingtin aggregates, and that these are toxic and could lead to disturbances of genetic transcription networks and mitochondrial dysfunctions.[32,33] Then, what are the mechanisms by which autophagy clears mutant huntingtin? Ultrastructural examination of huntingtin-transfected cells showed abundant accumulation of cathepsin

D-positive autophagic vacuoles with or without sequestered cellular constituents, dense lysosomes, and multilamellar and tubuloveseicular structures.[26] Ravikumar *et al.*[34] investigated whether autophagy can degrade mutant huntingtin with expanded polyQ repeats. Degradation of 74 polyQ repeats fused to the amino terminus of GFP (polyQ74-GFP) transfected into COS7 or PC12 cells was inhibited by 3-methyladenine, a specific inhibitor of autophagy, and enhanced by rapamycin. Rapamycin acts by inhibiting the mammalian target of rapamycin (mTor) kinase, which forms the core of a nutrient- and growth factor-sensitive complex that control protein synthesis, and suppresses autophagy.[35] Importantly, inhibitors of autophagy enhance cell death, whereas rapamycin prevents the effects. Furthermore, once the overexpressed polyQ74-GFP forms insoluble large aggregates, the insoluble aggregates become resistant to rapamycin-induced autophagy. The data clearly demonstrate that failure to degrade polyQ expansions by autophagy is associated with accelerated progression of HD and that stimulation of autophagy in the early stages of the disease by rapamycin treatment could prevent deposition of polyQ aggregates. Rapamycin enhances the autophagic clearance of different proteins with long polyQ and polyalanine (polyA)-expanded proteins, and reduces their neurotoxicity. Thus, rapamycin and its analogs can be potentially used therapeutically for neurodegenerative diseases caused by aggregate-prone proteins.[36] It has been shown that mTor is sequestered in polyQ aggregates in transgenic mice expressing mutant huntingtin and patient brains of HD. Sequestration of mTor in polyQ aggregates inhibits nuclear-cytoplasm shuttling of mTor, leading to inactivation of mTor.[37] The inactivation in turn induces autophagy. Hence, co-sequestration of aggregates with mTor leads to inhibition of mTor activity, which may provide a partial explanation for accumulation of autophagic vacuoles in neurodegenerative diseases. On the other hand, the activation of autophagy via an insulin signal pathway clears accumulated polyQ proteins independent of mTor, as reported by Yamamoto *et al.*[38] They found that aggregates of mutant huntingtin activate insulin receptor substrate-2 involving the signaling cascades of insulin and insulin-like growth factor 1. Such activation turns on class III PI3K to induce autophagy, thus contributing to clearance of huntingtin aggregates.[38]

Invariably, AD is the most prevalent form of neurodegenerative diseases with dementia and associates with extracellular deposition of beta-amyloid (Aβ). Presenilin-1 (PS1) is one of several proteins linked to early-onset familial AD, and together with PS2, plays a catalytic role in the γ-secretase complex necessary for intermediate proteolysis of the amyloid precursor protein (APP) followed by liberation of Aβ. Although it has been noticed that autophagic vacuoles accumulate in hippocampal and prefrontal cortical pyramidal neurons of Alzheimer-type dementia,[23,24] the mechanism remains unclear. Wilson *et al.*[39] found the formation of enlarged late endosome-like structures, including α- and β-synuclein, in the perikarya of PS1$^{-/-}$ primary neurons and hippocampal tissue of patients with the Levy body variant of AD. Formation of such organelles is rescued by exogenous expression of not only wild-type PS but also dominant-negative PS1 lacking its activity, indicating that PS1 has another function besides γ-secretase. Esselens *et al.*[40] demonstrated the accumulation of telencephalin, a neural specific intercellular adhesion molecule known to interact with PS1, in vacuoles positive for Atg12 and LC3, but not cathepsin D, in PS1$^{-/-}$ hippocampal neurons. Similar to the report of Wilson *et al*,[39] the formation of such vacuoles was suppressed by not only wild-type but also mutant PS1. Furthermore, Esselens *et al.*[40] used cathepsin D knockout mice to show the degradation of telencephalin in lysosomes. Collectively, these results suggest that PS1 might play important roles in autophagosome and lysosomal fusion step. Recently, Yu *et al.*[41] reported the role of autophagy in Aβ production. Their exhaustive electron and immunoelectron microscopic analyses revealed accumulation of LC3-positive autophagic vacuoles in brains of AD patients and in AD model mice, neural cell lines, and in a non-neural APP-expressing cell line, and also the localization of PS1, Aβ40, Aβ42, and necastrin on internal and limiting membrane components of autophagic vacuoles. Further, they found that induction of autophagy evoked Aβ production, and inversely, inhibition of autophagy suppressed Aβ production. Finally, they observed the PS1-dependent γ-secretase activity in biochemical isolated autophagic vacuoles. Based on these findings, they proposed a novel mechanism for the generation of Aβ via autophagy that emphasized the prominent role of autophagy in AD pathogenesis.[41]

PD is a neurodegenerative disorder associated with progressive loss of dopaminergic neurons of the substantia nigra and locus coeruleus. The major clinical symptoms of PD are body rigidity, hypokinesia, and postural instability associated with trembling extremities.[42] Pathological examination shows marked accumulation of cytoplasmic inclusions of proteinaceous material with lipids called Lewy bodies. Lewy bodies consist of lipids, ubiquitin, enzymes involved in ubiquitin-related pathways, neurofilament proteins, α-synuclein, synphilin-1, and other entangled proteins. Mutations in the gene encoding α-synuclein, which is localized in presynaptic terminals and is abundantly present in Lewy bodies, are identified in certain cases of familial PD.[43,44] α-Synuclein is a protein of unknown function and a major component of Lewy bodies. Among three point mutations in α-synuclein causing an autosomal dominant form of familial PD, two mutations of α-synuclein (A53T and A30P) have been studied extensively. These α-synuclein mutants have a stronger tendency to form fibrils than wild-type α-synuclein. Hence, similar to huntingtin with abnormal polyQ expansion, misfolded or aggregated α-synuclein is believed to cause cell toxicity and inhibits the ubiquitin-proteasome system. Lewy bodies may contribute to aggregation of α-synuclein into inclusions to moderate its toxicity.[45,46] It has been reported recently that autophagic-lysosomal dysfunction may be also involved in PD. Using stable PC12 transfectants expressing wild-type and A53T mutant α-synuclein, Stefanis *et al.*[47] showed that marked accumulation of autophagic vacuoles and impairment of lysosomal and ubiquitin-proteasome functions are principal phenotypes in the cells. On the other hand, clearance of mutant α-synuclein is strongly dependent on both ubiquitin-proteasomes and macroautophagy,[48] but not chaperone-mediated autophagy capable of degrading wild-type α-synuclein efficiently.[49]

Impairment of Autophagy in Neurons

Recently, our group and Mizushima's group investigated the pathophysiological roles of basal or constitutive autophagy in the brain.[50,51] For this purpose, we generated neuron-specific autophagy-deficient mice (*Atg7*$^{F/F}$:Nes mice) by crossing *Atg7*-conditional knockout mice (*Atg7*$^{F/F}$) with transgenic mice expressing the Cre recombinase under the control of the neuron-specific Nestin (Nes) promoter, Nes-*Cre*. We found that mice lacking Atg7 (i.e., autophagy) in the central nervous system exhibited various behavioral deficits, such as abnormal limb-clasping reflexes and reduction of coordinated movement, and died within 28 weeks after birth. Histological analysis showed that *Atg7*-deficiency was associated with neuronal loss in the cerebral and cerebellar cortices. Intriguingly, *Atg7*-deficient neurons showed abundant accumulation of polyubiquitylated proteins, which appeared as inclusion bodies whose size and number increased with aging (Figure 3), but had functionally intact proteasomes, whose impairment is generally known to cause abnormal ubiquitin-mediated proteolysis.[50] Hara *et al.*[51] also reported that almost all these phenotypes, if not all, were observed in neural-specific mice deficient in *Atg5*, another autophagy-essential gene. Thus, many of the critical symptoms seen in neural-specific autophagy-deficient mice are similar to those of patients with neurodegenerative disorders.

Histological analyses of the brains of *Atg7*$^{F/F}$:Nes mice revealed loss of specific neurons, such as pyramidal neurons in the cerebral cortex and hippocampus, and Purkinje cells in the cerebellum. Unexpectedly, immunohistological analysis using anti-ubiquitin antibody identified ubiquitin-positive proteinaceous aggregates throughout the brain, although the staining intensity varied from one region to another. Few ubiquitin-positive inclusions were recognized in brain regions with evident neuronal loss, whereas many ubiquitin inclusions were noted in areas with barely any neuronal loss such as the hypothalamus. Although we could not determine whether neuronal death is due to accumulation and subsequent inclusion formation of ubiquitylated proteins, neurons with large inclusions survived. Conversely, large pyramidal neurons and Purkinje cells seem vulnerable to ubiquitylated proteins and die before the formation of large inclusions. Whether the formation of inclusion bodies in neurons is protective or toxic is under debate, although emerging evidence emphasizes that protein aggregation can be a protective mechanism.[32,33]

Although accumulation of ubiquitylated proteins and cell death were noted in autophagy-deficient hepatocytes[14] and neurons,[50,51] such phenotypes were not observed in growing cells such as mouse embryonic fibroblasts (MEFs) and astroglial cells, irrespective of autophagy deficiency. Thus, it seems that autophagy is not required in rapidly dividing cells, at least with respect to multiplication of these cells. These results might also reflect the difference in autophagic activity among cell types. It is possible that the cell division cycle results in dilution of ubiquitylated proteins in autophagy-deficient MEFs, preventing their accumulation. Alternatively, other degradation pathways, such as chaperone-mediated autophagy, could contribute to degradation of long-lived proteins in growing MEFs. Considered together, it is clear that macroautophagy (the massive autophagy pathway discussed here) plays important roles in proteolysis in quiescent cells.

Autophagy deficiency is considered to result in delays of global turnover of cytoplasmic components, resulting in accumulation of misfolded and/or unfolded proteins followed by formation of inclusion bodies. However, a recent report showed that p62/SQSTM1 harboring a ubiquitin binding domain, interacted with LC3 and was degraded via autophagy.[52] We also obtained similar results and found that

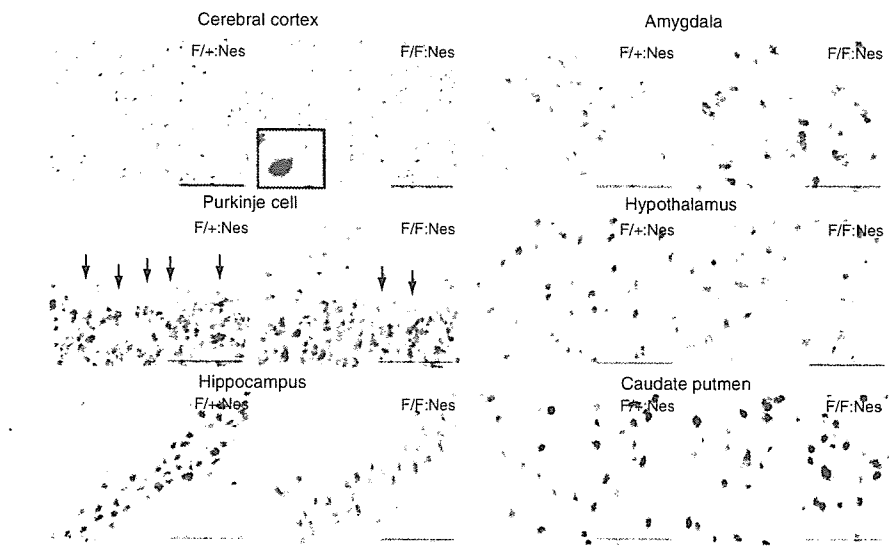

Figure 3 Ubiquitin-positive inclusions in autophagy-deficient neurons. The presence of ubiquitin-positive dots was examined immunohistochemically in several regions of the brain including cerebral cortex, cerebellum (Purkinje cells), hippocampus, amygdala, hypothalamus, caudate putamen of *Atg7*$^{F/+}$:Nes (left panels), and *Atg7*$^{F/F}$:Nes (right panels) mice. Note the presence of numerous ubiquitin dots in the amygdala and hypothalamus of representative mutants. Bars, 100 μm in the panel of cerebral cortex, and 50 μm in others

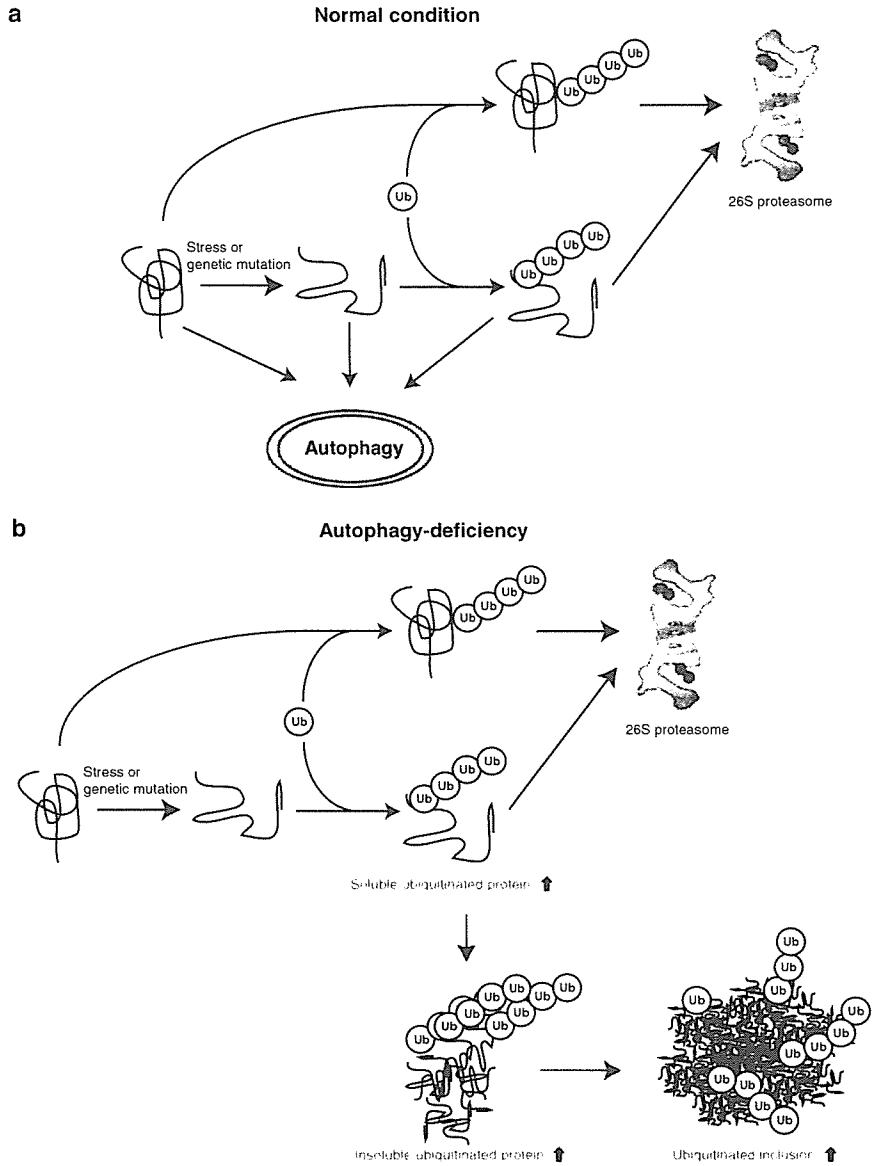

Figure 4 A schematic diagram of protein destruction pathways mediated by the proteasome and autophagy. The majority of cellular proteins, if not all, are polyubiquitylated before hydrolysis by the proteasome (an ATP-dependent proteolytic complex). Similarly, unfolded/misfolded proteins generated by environmental stresses or genetic mutations are discarded after polyubiquitylation by the same proteolytic system (**a**). Aging-related decline in autophagic activity causes accumulation of highly ubiquitylated proteins, which are recovered as both soluble and insoluble forms (**b**). As autophagy could feed both ubiquitylated and unubiquitylated protein(s), it is not clear at present whether polyubiquitylated aggregates/inclusions in autophagy-deficient neurons are formed consequent to impairment of degradation of unubiquitylated proteins or aggressively polyubiquitylated proteins. In addition, further work is needed to determine whether the two proteolytic systems (autophagy and proteasomes) work independently or cooperatively, and whether autophagy and the proteasome feed a similar set of normal and/or misfolded/unfolded proteins in general. Red text: protein dynamics associated with autophagy deficiency, Ub: ubiquitin

p62 plays a critical role in the formation of ubiquitin-positive aggregates by impaired autophagy (unpublished data). These results imply that ubiquitylated unfavorable proteins might be selectively sequestered into autophagosomes in part via p62 (which may retain its shuttling ability of ubiquitylated proteins). In either case (non-selective or selective degradation of ubiquitylated proteins by autophagy), our results indicate that autophagy operates not only as a supplier of amino acids under nutrient-poor conditions but also as a house cleaner of damaged proteins under nutrient-rich conditions.

Concluding Remarks

Considering the role of autophagy in neurodegenerative diseases, it is possible to align time-dependent enhancement and inactivation of autophagy. First, misfolded and/or

unfolded protein aggregates formed in neurons cause sequestration of mTor along with the aggregates, leading to significant inactivation of mTor, which stimulates autophagy (autophagosome formation). Second, if the size of aggregates is small enough and the degree of aggregation is moderate, the aggregates are engulfed into autophagosomal lumen and subsequently degraded via autophagy. Unless the amounts of aggregates surpass the clearance capacity of autophagosomes, maximal activation of autophagy by pharmaceutical agents such as rapamycin could be effective in preventing the progression of the disease. It is noteworthy that the expression of aggregation-prone protein(s) observed frequently in familial neurodegenerative disorders is not required for the formation of inclusions associated with impaired autophagy, suggesting the involvement of autophagy even in sporadic neurodegenerative diseases. On the other hand, autophagic activity of rat liver decreases with aging and this decrease conversely correlates with an increase in the accumulation of oxidized proteins.[36] Thus, age-dependent onset of neurodegenerative diseases most likely correlates with the age-dependent decline of autophagic activity. It is generally accepted that deficits of the proteasome-ubiquitin system are linked to various neurodegenerative disorders. Intriguingly, however, no obvious inhibition of the ubiquitin-proteasome system occurs in the mouse brain lacking autophagy, providing compelling evidence that constitutive autophagy plays a prominent role in neuronal survival, independent of proteasome function (Figure 4). In this context, we stress that proteasome inhibition induces augmented autophagy in order to eliminate unnecessary accumulated proteins, probably compensating the loss of proteasome functions.[22] Thus, the two major proteolytic pathways naturally differ in the cooperative responses in cells. We emphasize the importance of autophagy as a process with adaptive and flexible responses. Finally, a better understanding of basal or constitutive autophagy, which maintains basal activity of macroautophagy in neurons, may help in the design of new strategies to prevent neurodegenerative diseases.

1. Goldberg AL. Protein degradation and protection against misfolded or damaged proteins. *Nature* 2003; **426**: 895–899.
2. Levine B, Klionsky DJ. Development by self-digestion: molecular mechanisms and biological functions of autophagy. *Dev Cell* 2004; **6**: 463–477.
3. Cuervo AM. Autophagy: in sickness and in health. *Trends Cell Biol* 2004; **14**: 70–77.
4. Mizushima N, Ohsumi Y, Yoshimori T. Autophagosome formation in mammalian cells. *Cell Struct Funct* 2002; **27**: 421–429.
5. Takeshige K, Baba M, Tsuboi S, Noda T, Ohsumi Y. Autophagy in yeast demonstrated with proteinase-deficient mutants and conditions for its induction. *J Cell Biol* 1992; **119**: 301–311.
6. Mizushima N, Yamamoto A, Matsui M, Yoshimori T, Ohsumi Y. *In vivo* analysis of autophagy in response to nutrient starvation using transgenic mice expressing a fluorescent autophagosome marker. *Mol Biol Cell* 2004; **15**: 1101–1111.
7. Kabeya Y, Mizushima N, Ueno T, Yamamoto A, Kirisako T, Noda T *et al.* LC3, a mammalian homologue of yeast Apg8p, is localized in autophagosome membranes after processing. *EMBO J* 2000; **19**: 5720–5728.
8. Kabeya Y, Mizushima N, Yamamoto A, Oshitani-Okamoto S, Ohsumi Y, Yoshimori T. LC3, GABARAP and GATE16 localize to autophagosomal membrane depending on form-II formation. *J Cell Sci* 2004; **117**: 2805–2812.
9. Tanida I, Sou YS, Ezaki J, Minematsu-Ikeguchi N, Ueno T, Kominami E. HsAtg4B/HsApg4B/autophagin-1 cleaves the carboxyl termini of three human Atg8 homologues and delipidates microtubule-associated protein light chain 3- and GABAA receptor-associated protein-phospholipid conjugates. *J Biol Chem* 2004; **279**: 36268–36276.
10. Ichimura Y, Kirisako T, Takao T, Satomi Y, Shimonishi Y, Ishihara N *et al.* A ubiquitin-like system mediates protein lipidation. *Nature* 2000; **408**: 488–492.
11. Tanida I, Tanida-Miyake E, Ueno T, Kominami E. The human homolog of Saccharomyces cerevisiae Apg7p is a Protein-activating enzyme for multiple substrates including human Apg12p, GATE-16, GABARAP, and MAP-LC3. *J Biol Chem* 2001; **276**: 1701–1706.
12. Tanida I, Tanida-Miyake E, Komatsu M, Ueno T, Kominami E. Human Apg3p/Aut1p homologue is an authentic E2 enzyme for multiple substrates, GATE-16, GABARAP, and MAP-LC3, and facilitates the conjugation of hApg12p to hApg5p. *J Biol Chem* 2002; **277**: 13739–13744.
13. Mortimore GE, Hutson NJ, Surmacz CA. Quantitative correlation between proteolysis and macro- and microautophagy in mouse hepatocytes during starvation and refeeding. *Proc Natl Acad Sci USA* 1993; **80**: 2179–2183.
14. Komatsu M, Waguri S, Ueno T, Iwata J, Murata S, Tanida I *et al.* Impairment of starvation-induced and constitutive autophagy in Atg7-deficient mice. *J Cell Biol* 2005; **169**: 425–434.
15. Tsukada M, Ohsumi Y. Isolation and characterization of autophagy-defective mutants of Saccharomyces cerevisiae. *FEBS Lett* 1993; **333**: 169–174.
16. Kuma A, Hatano M, Matsui M, Yamamoto A, Nakaya H, Yoshimori T *et al.* The role of autophagy during the early neonatal starvation period. *Nature* 2004; **432**: 1032–1036.
17. Lum JJ, Bauer DE, Kong M, Harris MH, Li C, Lindsten T *et al.* Growth factor regulation of autophagy and cell survival in the absence of apoptosis. *Cell* 2005; **120**: 237–248.
18. Hollenbeck PJ. Products of endocytosis and autophagy are retrieved from axons by regulated retrograde organelle transport. *J Cell Biol* 1993; **121**: 305–315.
19. Puls I, Jonnakuty C, LaMonte BH, Holzbaur EL, Tokito M, Mann E *et al.* Mutant dynactin in motor neuron disease. *Nat Genet* 2003; **33**: 455–456.
20. Hafezparast M, Klocke R, Ruhrberg C, Marquardt A, Ahmad-Annuar A, Bowen S *et al.* Mutations in dynein link motor neuron degeneration to defects in retrograde transport. *Science* 2003; **300**: 808–812.
21. Ravikumar B, Acevedo-Arozena A, Imarisio S, Berger Z, Vacher C, O'Kane CJ *et al.* Dynein mutations impair autophagic clearance of aggregate-prone proteins. *Nat Genet* 2005; **37**: 771–776.
22. Iwata A, Riley BE, Johnston JA, Kopito RR. HDAC6 and microtubules are required for autophagic degradation of aggregated huntingtin. *J Biol Chem* 2005; **280**: 40282–40292.
23. Okamoto K, Hirai S, Iizuka T, Yanagisawa T, Watanabe M. Reexamination of granulovacuolar degeneration. *Acta Neuropathol (Berlin)* 1991; **82**: 340–345.
24. Cataldo AM, Hamilton DJ, Barnett JL, Paskevich PA, Nixon RA. Properties of the endosomal-lysosomal system in the human central nervous system: disturbances mark most neurons in populations at risk to degenerate in Alzheimer's disease. *J Neurosci* 1996; **16**: 186–199.
25. Anglade P, Vyas S, Javoy-Agid F, Herrero MT, Michel PP, Marquez J *et al.* Apoptosis and autophagy in nigral neurons of patients with Parkinson's disease. *Histol Histopathol* 1997; **12**: 25–31.
26. Kegel KB, Kim M, Sapp E, McIntyre C, Castano JG, Aronin N *et al.* Huntingtin expression stimulates endosomal-lysosomal activity, endosome tubulation, and autophagy. *J Neurosci* 2000; **20**: 7268–7278.
27. Petersen A, Larsen KE, Behr GG, Romero N, Przedborski S, Brundin P *et al.* Expanded CAG repeats in exon 1 of the Huntington's disease gene stimulate dopamine-mediated striatal neuron autophagy and degeneration. *Hum Mol Genet* 2001; **10**: 1243–1254.
28. Tanida I, Minematsu-Ikeguchi N, Ueno T, Kominami E. Lysosomal turnover, but not a cellular level, of endogenous LC3 is a marker for autophagy. *Autophagy* 2005; **1**: 84–91.
29. Nishino I, Fu J, Tanji K, Yamada T, Shimojo S, Koori T *et al.* Primary LAMP-2 deficiency causes X-linked vacuolar cardiomyopathy and myopathy (Danon disease). *Nature* 2000; **406**: 906–910.
30. Tanaka Y, Guhde G, Suter A, Eskelinen EL, Hartmann D, Lullmann-Rauch R *et al.* Accumulation of autophagic vacuoles and cardiomyopathy in LAMP-2-deficient mice. *Nature* 2000; **406**: 902–906.
31. Ikeda H, Yamaguchi M, Sugai S, Aze Y, Narumiya S, Kakizuka A. Expanded polyglutamine in the Machado–Joseph disease protein induces cell death *in vitro* and *in vivo*. *Nat Genet* 1996; **13**: 196–202.
32. Sanchez I, Mahlke C, Yuan J. Pivotal role of oligomerization in expanded polyglutamine neurodegenerative disorders. *Nature* 2003; **421**: 373–379.
33. Arrasate M, Mitra S, Schweitzer ES, Segal MR, Finkbeiner S. Inclusion body formation reduces levels of mutant huntingtin and the risk of neuronal death. *Nature* 2004; **431**: 805–810.
34. Ravikumar B, Duden R, Rubinsztein DC. Aggregate-prone proteins with polyglutamine and polyalanine expansions are degraded by autophagy. *Hum Mol Genet* 2002; **11**: 1107–1117.
35. Inoki K, Corradetti MN, Guan KL. Dysregulation of the TSC-mTOR pathway in human disease. *Nat Genet* 2005; **37**: 19–24.
36. Bergamini E. Autophagy: a cell repair mechanism that retards ageing and age-associated diseases and can be intensified pharmacologically. *Mol Aspects Med* 2006; **27**: 403–410.
37. Ravikumar B, Vacher C, Berger Z, Davies JE, Luo S, Oroz LG *et al.* Inhibition of mTOR induces autophagy and reduces toxicity of polyglutamine expansions in fly and mouse models of Huntington disease. *Nat Genet* 2004; **36**: 585–595.
38. Yamamoto A, Cremona ML, Rothman JE. Autophagy-mediated clearance of huntingtin aggregates triggered by the insulin-signaling pathway. *J Cell Biol* 2006; **172**: 719–731.
39. Wilson CA, Murphy DD, Giasson BI, Zhang B, Trojanowski JQ, Lee VM. Degradative organelles containing mislocalized alpha-and beta-synuclein proliferate in presenilin-1 null neurons. *J Cell Biol* 2004; **165**: 335–346.

40. Esselens C, Oorschot V, Baert V, Raemaekers T, Spittaels K, Serneels L *et al.* Presenilin 1 mediates the turnover of telencephalin in hippocampal neurons via an autophagic degradative pathway. *J Cell Biol* 2004; **166**: 1041–1054.
41. Yu WH, Cuervo AM, Kumar A, Peterhoff CM, Schmidt SD, Lee JH *et al.* Macroautophagy – a novel Beta-amyloid peptide-generating pathway activated in Alzheimer's disease. *J Cell Biol* 2005; **171**: 87–98.
42. Jenner P, Olanow CW. Understanding cell death in Parkinson's disease. *Ann Neurol* 1998; **44**: S72–S84.
43. Kruger R, Kuhn W, Muller T, Woitalla D, Graeber M, Kosel S *et al.* Ala30Pro mutation in the gene encoding alpha-synuclein in Parkinson's disease. *Nat Genet* 1998; **18**: 106–108.
44. Polymeropoulos MH, Lavedan C, Leroy E, Ide SE, Dehejia A, Dutra A *et al.* Mutation in the alpha-synuclein gene identified in families with Parkinson's disease. *Science* 1997; **276**: 2045–2047.
45. Chung KK, Dawson VL, Dawson TM. The role of the ubiquitin-proteasomal pathway in Parkinson's disease and other neurodegenerative disorders. *Trends Neurosci* 2001; **24**: S7–S14.
46. Mouradian MM. Recent advances in the genetics and pathogenesis of Parkinson disease. *Neurology* 2002; **58**: 179–185.
47. Stefanis L, Larsen KE, Rideout HJ, Sulzer D, Greene LA. Expression of A53T mutant but not wild-type alpha-synuclein in PC12 cells induces alterations of the ubiquitin-dependent degradation system, loss of dopamine release. and autophagic cell death. *J Neurosci* 2001; **21**: 9549–9560.
48. Webb JL, Ravikumar B, Atkins J, Skepper JN, Rubinsztein DC. Alpha-Synuclein is degraded by both autophagy and the proteasome. *J Biol Chem* 2003; **278**: 25009–25013.
49. Cuervo AM, Stefanis L, Fredenburg R, Lansbury PT, Sulzer D. Impaired degradation of mutant alpha-synuclein by chaperone-mediated autophagy. *Science* 2004; **305**: 1292–1295.
50. Komatsu M, Waguri S, Chiba T, Murata S, Iwata J, Tanida I *et al.* Loss of autophagy in the central nervous system causes neurodegeneration in mice. *Nature* 2006; **441**: 880–884.
51. Hara T, Nakamura K, Matsui M, Yamamoto A, Nakahara Y, Suzuki-Migishima R *et al.* Suppression of basal autophagy in neural cells causes neurodegenerative disease in mice. *Nature* 2006; **441**: 885–889.
52. Bjorkoy G, Lamark T, Brech A, Outzen H, Perander M, Overvatn A *et al.* p62/SQSTM1 forms protein aggregates degraded by autophagy and has a protective effect on huntingtin-induced cell death. *J Cell Biol* 2005; **171**: 603–614.

BRAIN RESEARCH 1073–1074 (2006) 93–102

available at www.sciencedirect.com

SCIENCE DIRECT®

www.elsevier.com/locate/brainres

BRAIN RESEARCH

Short Communication

Localization of Id2 mRNA in the adult mouse brain

Kazuhito Kitajima[a,b,c], *Ryosuke Takahashi*[c], *Yoshifumi Yokota*[a,*]

[a]*Department of Molecular Genetics, School of Medicine, University of Fukui, 23-3 Shimoaizuki, Matsuoka, Fukui 910-1193, Japan*
[b]*Department of Neurology, Fukui Red Cross Hospital, 2-4-1 Tsukimi, Fukui 918-8501, Japan*
[c]*Department of Neurology, Graduate School of Medicine, Kyoto University, 54 Shogoin Kawahara-cho, Sakyo 606-8507, Kyoto, Japan*

ARTICLE INFO

Article history:
Accepted 12 December 2005
Available online 27 January 2006

Keywords:
Helix–loop–helix protein
Id2
Gene expression
Adult brain
Mouse

Abbreviations:
bHLH, basic helix–loop–helix
HLH, helix–loop–helix
DEPC, diethylpyrocarbonate

ABSTRACT

Id proteins are negative regulators of basic helix–loop–helix transcription factors and are involved in cellular differentiation and proliferation. Four members of the Id gene family exhibit closely related but distinct expression patterns in various mammalian organs of not only embryos but also adults. Among them, Id2 is known to be expressed in Purkinje cells and neurons in the cortical layers of the adult mouse brain, suggesting that Id2 is involved in some neural functions in the adult. To get insight into the role of Id2 in the nervous system, we investigated the localization of Id2 mRNA-expressing cells in the adult mouse brain in detail by in situ hybridization with the radiolabeled antisense probe and compared it with the localization of other Id gene family members. The results indicated that Id2 mRNA is detected in more varied brain regions than previously reported. These regions include the amygdaloid complex, caudate putamen, globus pallidus, substantia nigra pars reticulata, suprachiasmatic nucleus, and the anterior part of the subventricular zone. These results suggest the possibility that Id2 plays a role in the neural activity and cognitive functions. On the other hand, Id1 was barely detectable. Although moderate or low expression of Id3 was observed diffusely, high expression was observed in some specific regions including the molecular layer of the dentate gyrus and the external capsule. Id4 mRNA was detected in the regions such as the caudate putamen and the lateral amygdaloid nucleus. Thus, the expression pattern of Id2 is distinct from those of other Id gene family members.

Transcription factors play essential roles in various biological processes including cellular differentiation and proliferation by regulating gene expression. They are categorized according to their structural similarities. The basic helix–loop–helix (bHLH) protein family is a typical example. The members of this family share structural characteristics of the basic region and the helix–loop–helix (HLH) domain, which are required for DNA binding and dimerization, respectively (Massari and Murre, 2000). In general, tissue-specific bHLH factors form heterodimers with ubiquitously expressed bHLH factors, so-called E proteins consisting of E2A gene products (E12 and E47), HEB and E2-2, and regulate the expression of their respective target genes via the consensus-binding site, the E box (Massari and Murre, 2000). Tissue-specific bHLH factors that exhibit a high degree of sequence conservation constitute subfamilies and are involved in similar biological processes (Kageyama and Nakanishi, 1997; Massari and Murre, 2000). For example, neurogenic bHLH factors, such as NeuroD and Mash1, play

Corresponding author. Fax: +81 776 61 8164.
E-mail address: yyokota@fmsrsa.fukui-med.ac.jp (Y. Yokota).

0006-8993/$ – see front matter © 2005 Elsevier B.V. All rights reserved.
doi:10.1016/j.brainres.2005.12.048

important roles in cell fate determination, specification and proliferation control during neurogenesis in a wide variety of species by constituting gene regulatory cascades and carrying out their specific functions (Kageyama and Nakanishi, 1997; Massari and Murre, 2000).

Id proteins, inhibitors of DNA binding/differentiation, are negative regulators of bHLH transcription factors, and four members of this protein family, Id1–Id4, have been identified in mammals (Massari and Murre, 2000; Ruzinova and Benezra, 2003). They possess HLH domains and form heterodimers with bHLH factors, but the resultant heterodimers are unable to bind DNA due to the lack of a DNA-binding domain in Id proteins (Massari and Murre, 2000; Ruzinova and Benezra, 2003). Thus, Id proteins inhibit the functions of bHLH factors in a dominant negative manner and suppress bHLH factor-dependent cellular differentiation (Massari and Murre, 2000; Ruzinova and Benezra, 2003). On the other hand, Id proteins have the ability to stimulate cell cycle progression. Although the mechanism remains unclear, Id proteins have been reported to have abilities to inhibit the enhanced expression of cyclin-dependent inhibitors such as p21 by bHLH factors and to antagonize the activity of Rb family proteins (Ruzinova and Benezra, 2003; Yokota and Mori, 2002). Based on these functional characteristics, Id proteins are thought to be involved in the regulation of cell differentiation and in the expansion of immature cell populations (Ruzinova and Benezra, 2003; Yokota and Mori, 2002). In fact, each member of the Id gene family is expressed in a wide range of embryonic tissues including the central nervous system, and different members show similar but distinct expression patterns (Andres-Barquin et al., 2000; Jen et al., 1996, 1997; Neuman et al., 1991; Rubenstein et al., 1999; Tzeng and de Vellis, 1998). Id genes are also expressed in the adult central nervous system (Andres-Barquin et al., 2000; Elliott et al., 2001; Neuman et al., 1991; Riechmann et al., 1994; Rubenstein et al., 1999; Tzeng and de Vellis, 1998), although there is a tendency for the expression levels to decrease (Andres-Barquin et al., 2000; Neuman et al., 1991; Tzeng and de Vellis, 1998). For example, Id2 is expressed in neurons in all layers of the cerebral cortex except layer 4, Purkinje cells of the cerebellum, the olfactory bulb (the mitral cell, glomerular and internal granule cell layers), the hippocampus, and the suprachiasmatic nucleus (SCN) of the adult rodent brain (Andres-Barquin et al., 2000; Elliott et al., 2001; Neuman et al., 1991; Rubenstein et al., 1999; Tzeng and de Vellis, 1998; Ueda et al., 2002). These observations suggest that Id proteins are involved in cellular functions in terminally differentiated and non-dividing cells, in addition to playing roles in cell differentiation and proliferation control.

To get insight into the role of Id2 in neural functions, we investigated the distribution of Id2 mRNA in the adult mouse brain by in situ hybridization. Adult male mice of ICR or the mixed genetic background between NMRI and 129/Sv were used in this study. Similar results were obtained from the two strains. Mice were deeply anesthetized with diethyl ether and perfused transcardially with PBS followed by fixative containing 4% paraformaldehyde in PBS. After perfusion, the brain was taken out of the skull, immersed in the same fixative for 24 h at 4 °C, transferred to 0.1% diethylpyrocarbonate (DEPC)-treated 20% sucrose in PBS for 48 h at 4 °C, and then frozen with OCT compound at −80 °C. The brain was cut into 10- m-thick sections on a cryostat and mounted on glass slides. Sections were stored at −80 °C until use. All animal procedures were performed in accordance with the guidelines of the University of Fukui for animal experiments. In situ hybridization was performed as described (Ishii et al., 1990; Mori et al., 2000). Briefly, 10- m-thick coronal sections were treated with 5 g/ml proteinase K and acetylated before hybridization. An ^{35}S-labeled RNA probe spanning nt 61–759 of the mouse Id2 cDNA was generated by transcription with RNA polymerase using the pBS-Id2 plasmid as template (Mori et al., 2000). The sections were hybridized in the presence of 50% formamide at 60 °C overnight, washed at high stringency, dipped with NTB2 emulsion (Kodak), and autoradiographed. The sections were then counterstained with the Cresyl Fast Violet solution to allow morphological identification. Anatomical determinations were made according to a standard atlas (Paxinos and Franklin, 2001). In situ hybridization of brain sections with the ^{35}S-labeled sense probe gave no appreciable signal and confirmed the specificity of the ^{35}S-labeled antisense probe for the detection of the Id2 mRNA (data not shown).

In the main olfactory bulb, Id2 mRNA was expressed in the mitral, glomerular, and granule cell layers (Mi, Gl, GrO) (Fig. 1A and Table 1), as reported (Neuman et al., 1991). In the anterior olfactory nucleus, both medial (AOM) and posterior (AOP) parts were stained (Fig. 1B). In the septum, Id2 mRNA was moderately expressed in the lateral septal nucleus, intermediate and ventral part (LSI and LSV, respectively) (Fig. 1C), although the expression level was lower in the lateral septal nucleus, dorsal part (LSD), and medial septal nucleus (MS) (Fig. 1C). Some Id2-expressing cells were distributed in the corpus callosum (cc) (Figs. 1C, 3E), in accordance with the report about Id2 mRNA expression in S100$^+$GFAP$^+$ astrocytes and GFAP$^-$ and O4$^-$ cells in the rat corpus callosum (Tzeng and de Vellis, 1998).

In the cerebral cortex, Id2 mRNA was detected in all layers except layer 4, and scattered cells were positive for Id2 mRNA in layer 1 (Figs. 1B–G, 2A–C). Strong Id2 mRNA expression was observed in layer 5 of the neocortex as reported (Figs. 1C–F) and in layer 2 in the piriform cortex (Pir) (Figs. 1B–D). In the cingulate (Cg/RS) and retrosplenial cortices (RS), the level of Id2 mRNA expression was high in layers 2 and 3 (Figs. 1E and F).

Strong expression of Id2 mRNA was observed in the many regions of the amygdaloid complex: the basolateral amygdaloid nucleus anterior part (BLA), lateral amygdaloid nucleus dorsolateral part (LaDL), ventromedial part (LaVM), ventrolateral part (LaVL), medial amygdaloid nucleus posterodorsal part (MePD), posteroventral part (MePV), posteromedial cortical amygdaloid nucleus (PMCo), and intercalated nuclei of the amygdala (I) (Figs. 1D–G and 3A). In the other subnuclei, moderately expressing cells were distributed (Fig. 3A). In addition, moderate expression was observed in the dorsal and ventral parts of the anterior amygdaloid area (AAD, AAV), anterior cortical amygdaloid nucleus (ACo), and nucleus of the lateral olfactory tract (LOT) (Fig 1D). High expression was also seen in the dorsal endopiriform nucleus (DEn) (Figs. 1B and F, 3A). Moderate expression was also observed in the bed nucleus of stria terminalis (BST) (Fig. 1D) and the intraamygdaloid division of the bed nucleus of the stria terminalis

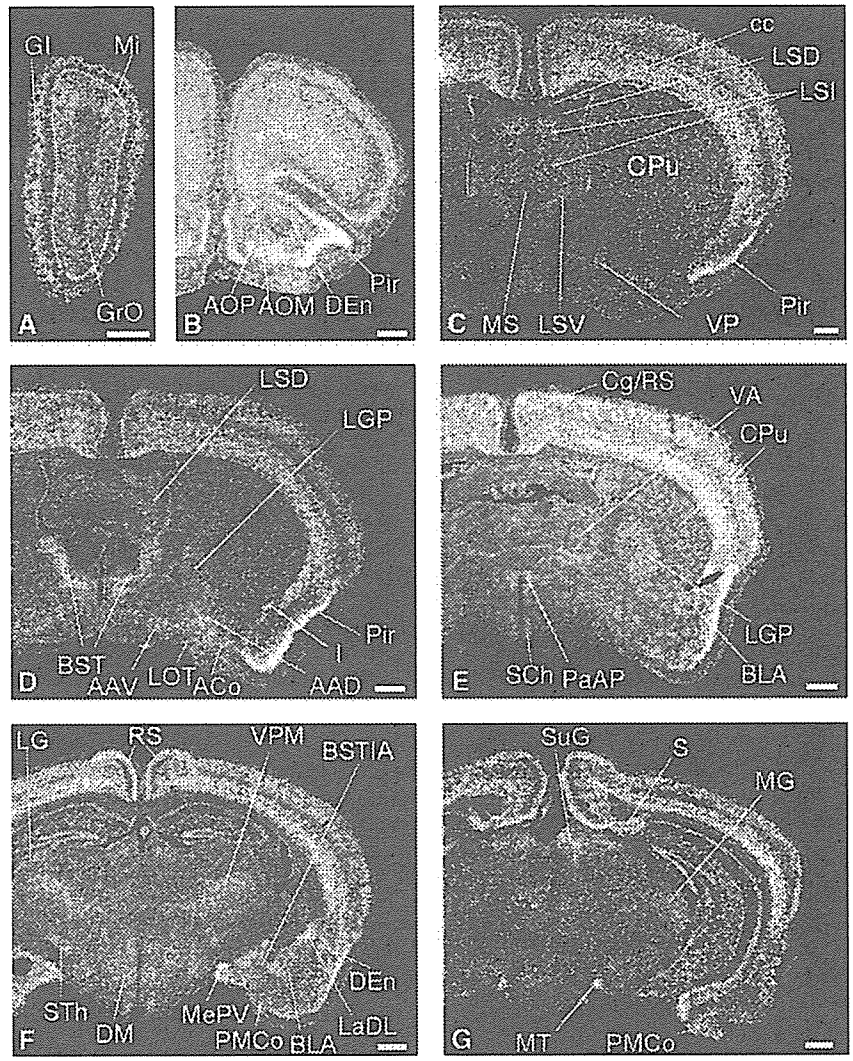

Fig. 1 – Expression of Id2 mRNA in the forebrain and thalamus. Dark field photomicrographs showing Id2 mRNA expression in coronal sections. Strong expression was observed in the piriform cortex (B) (C), bed nucleus of the stria terminalis, intercalated nuclei of the amygdala (D), cingulate/retrosplenial cortex (E), dorsal endopiriform nucleus, lateral amygdaloid nucleus dorsolateral part, medial amygdaloid nucleus posterodorsal part (F), subiculum, superficial gray layer of the superior colliculus, and medial terminal nucleus of the accessory optic tract (G). Scale bar, 500 m. Abbreviations are listed in Table 1.

(BSTIA) (Fig. 1F). Cells expressing Id2 mRNA moderately or strongly were dispersed throughout the hippocampus. It has been reported that Id2-expressing cells in the hippocampus are interneurons and/or glial cells (Elliott et al., 2001). Id2 positive cells were found in subgranular zone (SGZ) of the dentate, but most of the granule cells and pyramidal cells were not labeled (Fig. 3B). Id2 mRNA was clearly detectable in the subiculum (S) (Figs. 1G, 2A and B). Macroscopic observation of the sections demonstrated that the globus pallidus showed the strongest reactivity in the basal ganglia. In the microscopic study of the globus pallidus, most cells were moderately labeled for Id2 mRNA (LGP) (Fig. 1E). Although medium- to large-sized neurons and some glial cells were moderately labeled in the caudate putamen, the majority of striatal neurons were not positive for Id2 expression (Figs. 1C–E and 3C).

In the subventricular zone (SVZ) and ependymal region, some cells were labeled (Fig. 3E). In the anterior part of the subventricular zone (SVZa), which is a source of neuronal progenitor cells for the olfactory bulb (Luskin, 1993), strongly labeled cells were detected (Fig. 3F). In ventral pallidum (VP), moderately labeled cells were detected (Fig. 1C).

Id2 mRNA was expressed in some thalamic subnuclei: moderate expression was seen in the ventral anterior thalamic nucleus (VA) and ventral posteromedial thalamic nucleus (VPM) and weak expression in other regions (Figs. 1E and F). Moderate Id2 expression was detected in the lateral and medial geniculate nucleus (LG, MG) (Figs. 1F and G) and in the subthalamic nucleus (STh) (Fig. 1F). Id2 mRNA was also moderately expressed in the suprachiasmatic nuclei (SCh) (Figs. 1E and 3D), paraventricular hypothalamic nucleus anterior parvicellular part (PaAP) (Fig. 1E), and dorsomedial hypothalamic nucleus (DM) (Fig. 1F). In other nuclei located in this area, the expression level was weak or undetectable (Fig. 1E).

Table 1 – Abbreviations

3N	Oculomotor nucleus
4N	Trochlear nucleus
10N	Dorsal motor nucleus of vagus
12N	Hypoglossal nucleus
AAD	Anterior amygdaloid area, dorsal part
AAV	Anterior amygdaloid area, ventral part
aci	Anterior commissure, intrabulbar part
ACo	Anterior cortical amygdaloid nucleus
AOM	Anterior olfactory nucleus, medial part
AOP	Anterior olfactory nucleus, posterior part
BLA	Basolateral amygdaloid nucleus, anterior part
BST	Bed nucleus of the stria terminalis
BSTIA	Bed nucleus of the stria terminalis, intraamygdaloid division
cc	Corpus callosum
cg	Cingulum
Cg/RS	Cingulate/retrosplenial cortex
CPu	Caudate putamen
DC	Dorsal cochlear nucleus
DEn	Dorsal endopiriform nucleus
DM	Dorsomedial hypothalamic nucleus
DR	Dorsal raphe nucleus
DRD	Dorsal raphe nucleus, dorsal part
DRV	Dorsal raphe nucleus, ventral part
ec	External capsule
Gl	Glomerular layer of the olfactory bulb
GrO	Granular cell layer of the olfactory bulb
hbc	Habenular commissure
I	Intercalated nuclei of the amygdala
ic	Internal capsule
InG	Intermediate gray layer of the superior colliculus
Int	Interposed cerebellar nucleus,
IP	Interpeduncular nucleus
IPL	Interpeduncular nucleus, lateral subnucleus
IPR	Interpeduncular nucleus, rostral subnucleus
LaDL	Lateral amygdaloid nucleus, dorsolateral part
Lat	Lateral dentate cerebellar nucleus
LaVL	Lateral amygdaloid nucleus, ventrolateral part
LaVM	Lateral amygdaloid nucleus, ventromedial part
LG	Lateral geniculate nucleus
LGP	Lateral globus pallidus
ll	Lateral lemniscus
LOT	Nucleus of the lateral olfactory tract
LPGi	Lateral paragigantocellular nucleus
LSD	Lateral septal nucleus, dorsal part
LSI	Lateral septal nucleus, intermediate part
LSO	Lateral superior olive
LSV	Lateral septal nucleus, ventral part
LVe	Lateral vestibular nucleus
MePD	Medial amygdaloid nucleus, posterodorsal part
MePV	Medial amygdaloid nucleus, posteroventral part
MG	Medial geniculate nucleus
MHb	Medial habenular nucleus
Mi	Mitral cell layer of the olfactory bulb
MnR	Median raphe nucleus
Mo5	Motor trigeminal nucleus
Mol	Molecular layer of the dentate gyrus
MS	Medial septal nucleus
MT	Medial terminal nucleus of the accessory Optic tract
PaAP	Paraventricular hypothalamic nucleus, anterior parvicellular part
PAG	Periaqueductal gray
Pir	Piriform cortex
PMCo	Posteromedial cortical amygdaloid nucleus (C3)
Pn	Pontine nuclei
PnO	Pontine reticular nucleus, oral part
Po	Posterior thalamic nuclear group
PO	Periolivary region
Pr5	Principal sensory trigeminal nucleus
RMC	Red nucleus, magnocellular part
RPO	Rostral periolivary region
RS	Retrosplenial cortex
RVL	Rostroventrolateral reticular nucleus
S	Subiculum
SCh	Suprachiasmatic nucleus
sm	Stria medullaris of the thalamus
SNR	Substantia nigra, reticular part
Sp5	Spinal trigeminal nucleus
st	Stria terminalis
STh	Subthalamic nucleus
SuG	Superficial gray layer of the superior colliculus
TS	Triangular septal nucleus
Tz	Nucleus of the trapezoid body
VA	Ventral anterior thalamic nucleus
VC	Ventral cochlear nucleus
VP	Ventral pallidum
VPL	Ventral posterolateral thalamic nucleus
VPM	Ventral posteromedial thalamic nucleus

While most cells in the pars reticulata of the substantia nigra (SNR) were moderately labeled for Id2 mRNA, no signals were detected in the pars compacta, pars lateralis, or ventral tegmental area (Fig. 2A). Moderate expression was observed in the interpeduncular nucleus (IP) (Fig. 2A). Strongly labeled cells were seen in the medial terminal nucleus of the accessory optic tract (MT) (Fig. 1G). Moderate Id2 mRNA expression was detected in the red nucleus, magnocellular part (RMC) (Fig. 2A). Id2 mRNA was expressed moderately in the superficial gray layer of the superior colliculus (SuG) and weakly in the oculomotor nucleus (3N), the trochlear nucleus (4N) and the intermediate gray layer of the superior colliculus (InG) (Figs. 2A and B).

In the pons, Id2 mRNA was strongly expressed in the pontine nucleus (Pn), while weak expression was observed in the median raphe nucleus (MnR), dorsal raphe nucleus (DR), periaqueductal gray (PAG), and pontine reticular nucleus, oral part (PnO) (Fig. 2B). Id2 mRNA was expressed strongly in the nucleus of lateral lemniscus (ll), rostral periolivary region (RPO), and the ventral and dorsal cochlear nuclei (VC, DC) and moderately in the nucleus of the trapezoid body (Tz), lateral superior olive (LSO), and periolivary region (PO) (Figs. 2C, D, and E). Id2 mRNA was weakly expressed in the motor trigeminal nucleus (Mo5) and principal sensory trigeminal nucleus (Pr5) (Fig. 2D). In the medulla, moderately labeled cells were found in the dorsal motor nucleus of the vagus (10N) (Fig. 2F). Id2 mRNA was weakly expressed in the hypoglossal nucleus (12N), lateral paragigantocellular nucleus (LPGi), spinal trigeminal nucleus (Sp5), and rostroventrolateral reticular nucleus (RVL) (Fig. 2F) In the cerebellum, Id2 was strongly expressed in Purkinje cells, but not in the external granule, molecular, or internal granule cell layers at 8 weeks old of age (Fig. 2E). The cells in the cerebellar nuclei (Int, Lat) showed moderate expression of Id2 mRNA (Fig. 2E). The lateral vestibular nucleus (LVe) displayed moderate expression of Id2 (Fig. 2E).

Northern blot analysis has revealed that the expression level of Id2 in the adult mouse brain is similar to that in the embryonic brain (Andres-Barquin et al., 2000; Neuman et al.,